

Natural infection of *C. elegans* by an oomycete reveals a new pathogen-specific immune response

Guled A. Osman^{1,2}, Michael K. Fasseas^{1,2}, Sneha L. Koneru¹, Clara L. Essmann³, Kyros Kyrou¹, Mandayam A Srinivasan^{3,4}, Gaotian Zhang⁵, Peter Sarkies^{6,7}, Marie-Anne Félix⁵ and Michalis Barkoulas^{1, *}

¹ Department of Life Sciences, Imperial College, London SW7 2AZ, United Kingdom.

² These authors contributed equally to this work.

³ Department of Computer Science, University College London, Engineering Building, Malet Place, London, WC1E 7JG, UK.

⁴ Department of Mechanical Engineering and Research Laboratory of Electronics, Massachusetts Institute of Technology, Cambridge, MA 02139, USA.

⁵ Institute of Biology of the Ecole Normale Supérieure (IBENS), CNRS, Inserm, 75005 Paris, France.

⁶ MRC London Institute of Medical Sciences, London, W12 0NN, United Kingdom.

⁷ Institute of Clinical Sciences, Imperial College London, W12 0NN, United Kingdom.

* Corresponding Author and Lead Contact: m.barkoulas@imperial.ac.uk

Running title: Natural infection of *C. elegans* by an oomycete pathogen

Keywords: oomycete; innate immunity; chitinase-like; chitolectins; *Myzocytiopsis humicola*; *C. elegans*; hypodermis; cuticle; pseudoenzymes

Summary

In its natural habitat, the nematode *Caenorhabditis elegans* encounters a plethora of other organisms, including many that are pathogenic [1,2]. The study of interactions between *C. elegans* and various pathogens has contributed to characterising key mechanisms of innate immunity [2–4]. However, how *C. elegans* recognises different pathogens to mount pathogen-specific immune responses remains still largely unknown [3,5–8]. Expanding the range of known *C. elegans*-infecting pathogens and characterising novel pathogen-specific immune responses are key steps towards answering this question. We report here that the oomycete *Myzocytiopsis humicola* is a natural pathogen of *C. elegans* and we describe its infection strategy. We identify a new host immune response to pathogen exposure, which involves induction of members of a previously uncharacterised gene family encoding chitinase-like (CHIL) proteins. We demonstrate that this response is highly specific against *M. humicola* and antagonises the infection. We propose that CHIL proteins may diminish the ability of the oomycete to infect by hindering pathogen attachment to the host cuticle. This work expands our knowledge of *C. elegans* natural eukaryotic pathogens and introduces a new pathosystem to address how animal hosts recognise and respond to oomycete infections.

Results and discussion

While collecting samples in Lisbon, we recovered a new isolate of *C. elegans* (strain JU2519) showing signs of a putative infection (Figure 1A). The most pronounced symptom was the appearance of pearl-like structures, which filled the entire body of the animal (Figures 1A and S1A). Based on the size of these structures (mean diameter $22.9 \mu\text{m} \pm 4.6 \text{ SEM}$) and the presence of distinct nuclei (Figure S1B), we hypothesised that the nematodes were facing a eukaryotic, perhaps fungal-like infection. To elucidate the identity of the pathogen we performed *Cox2*, 18S and ITS sequencing and identified the organism as an oomycete, genetically most similar to *Myzocytiopsis humicola* (99.9% similarity in 18S, 93.6% in *Cox2* and 88.3% in ITS sequence, Figures S1C, S1D and Data S1). Oomycetes morphologically resemble fungi yet they are evolutionary distinct and belong to the heterokonts, a eukaryotic clade that also includes brown algae and diatoms [9]. Oomycetes can infect a range of animals and plants. While plant pathogenic oomycetes, such as the potato blight pathogen *Phytophthora infestans*, have been widely studied [10,11], research on animal pathogenic oomycetes has been more limited, largely due to the paucity of experimentally tractable hosts [12]. Previous studies had provided morphological descriptions of *Myzocytiopsis* species [9,13], however, such nematode infections were never explored at the molecular level and there was no prior evidence that *C. elegans* could be infected by an oomycete naturally or under lab conditions. Therefore, we sought to establish a new pathosystem to model oomycete infections using *C. elegans* as a host.

We first characterised how the pathogen grows inside the *C. elegans* lab reference N2. Each nematode contained a mean of 184 ± 20 sporangia at the final stage of infection (Figure 1B). The sporangia initially contain undifferentiated

cytoplasmic mass and differentiate to produce infectious zoospores (16 ± 4 zoospores per sporangium, Figures 1C and 1D). The zoospores are known to be biflagellate and motile [13,14] and differentiate within the sporangia until released through an evacuation tube (Figure 1C). The released zoospores encyst and develop adhesive buds (Figure 1E), which attach to the nematode cuticle (Figure 1F). The pathogen penetrates inside (Figure 1G) and spreads in the form of a narrow hypha (Figure 1H), which swells and partitions into distinct sporangia (Figure 1I). The growth of hyphae and development of sporangia happen exclusively within the nematode. This characterisation was fully consistent with what was previously reported for *M. humicola* infections of other rhabditid nematodes [13,14]. Therefore, the Lisbon isolate is indistinguishable from *M. humicola* with regard to the morphology of sticky buds, zoospores, sporangia and the strategy of zoospore release [13,14]. Although *M. humicola* has been reported to be able to undergo both sexual and asexual reproduction [13,14], we only observed an asexual life cycle in our lab culture conditions.

To validate further the pathogen identification, we used fluorescent *in situ* hybridisation (FISH) using a probe targeting transcripts of the *M. humicola* 18S and L30 ribosomal protein genes. We were able to detect the oomycete both at early stages while entering the host, and at later stages when growing in the form of hypha within the nematode body, leading to the development of sporangia (Figures 1J-1M). Taken together with our genetic and morphological characterisation, we conclude that the Lisbon oomycete is a new isolate of *M. humicola*.

To address whether there is any spatial specificity for pathogen entry through the cuticle, we visualized pathogen attachment via scanning electron microscopy. We observed that *M. humicola* attachment is specific to the mouth and the longitudinal

ridges of the cuticle, known as alae (Figures 1N and 1O). The specific attachment to the alae is rather unusual since bacterial or fungal pathogens commonly attach over the entire surface of the cuticle, or adhere to the mouth, vulva or the rectum [2].

To study the underlying mechanisms of infection and immunity in a controlled manner as previously done for other pathogens [15], we established an assay to quantify how many animals showed symptoms of oomycete infection over time. In this assay, 50 synchronised fourth larval stage (L4) nematodes are exposed to 3 infected animals per plate for a total period of 48 hours (Figure 2A). The animals are monitored for the number of newly infected nematodes and transferred to new plates every 24 hours to ensure food availability for a period of up to 7 days. We found that *M. humicola* infections were more rapid at 25°C as opposed to the standard *C. elegans* growth temperature of 20°C (Figure 2B). We also found that *M. humicola* showed some host specificity and could infect all tested *Caenorhabditis* species and *Oscheius tipulae*, but not *Pristionchus pacificus* (Figure S1E).

We then asked whether mutants impaired for some conserved innate immunity pathway component, or showing defects in cuticle formation were more susceptible to oomycete infections. We found that mutations attenuating the conserved p38 MAPK pathway, previously implicated in *C. elegans* immunity to bacterial or fungal pathogens [16–18] also led to a higher sensitivity to oomycete infections (Figures 2C and 2D). In addition, we found that mutations in the nucleotide sugar transporter *srf-3* that alter the surface antigenicity of the cuticle [19,20], led to increased host sensitivity to infections (Figures 2E and 2F). Although in these assays we score infected animals based on symptoms and not survival (see STAR Methods), there was a marginal difference in survival of these mutants on non-pathogenic *E. coli* (Figures

2D and 2F), so the reduced resistance to the pathogen could in part reflect a more general problem of fitness.

To characterise the transcriptional response to infection, we used the established infection assay combined with RNA sequencing (RNA-seq) to study changes in expression in N2 and JU2519 at 12 and 24 hours post exposure to *M. humicola* in comparison to control treatments devoid of the pathogen. We identified genes differentially expressed in N2 and JU2519 (Data S2). In general, the statistically significant changes in gene expression post exposure to *M. humicola* were modest in magnitude, possibly reflecting the moderate rate of animal infection. Divergent pathogens could trigger a shared host response, as previously shown for microsporidia and nodaviruses, both intracellular pathogens of *C. elegans* that infect intestinal cells [6,21,22]. We compared the transcriptional response to *M. humicola* exposure to the response to infection by other pathogens. Overall, we found limited overlap between our data and 42 other gene sets, as in most cases less than 10% of highly responding genes to other microbes were also present in our data (Data S3, see overlap tab). Interestingly, even when comparing to the response against *Drechmeria coniospora*, a fungus that infects through the cuticle like *M. humicola*, the overlap was still limited (Fig. 3A). Gene set enrichment analysis of genes upregulated in JU2519 suggested a significant intersection (NOM p value <0.05 and FDR < 0.25) with 1 out of 42 gene sets at 12 hours and 10 out of 42 gene sets at 24 hours (Data S3, see GSEA tab, note that no significant intersection was found for N2). In most cases, this significant intersection consisted of a limited number of genes (Data S3, see genes GSEA tabs). For example, genes upregulated in JU2519 at 24 hours showed significant intersection with genes upregulated upon infection with *D. coniospora*. This overlap contained anti-microbial peptides belonging to the *neuropeptide-like*

(*nlp*) and *caenacin* (*cnc*) gene families, previously shown to be upregulated upon fungal infections and cuticle damage [23,24] (Data S3, see genes GSEA JU2519_24h). Genes upregulated in JU2519 at 12 and 24 hours also showed a significant intersection with genes upregulated upon infection of nematodes with the microsporidia *Nematocida parisii* or the Orsay virus (Data S3, see genes GSEA tabs). This overlap contained members of the *pals* gene family, previously shown to be a hallmark of microsporidia and viral infections [21,22,25,26]. Taken together, these results suggest that the transcriptional response to *M. humicola* shows some limited shared aspects with the response to infection by other pathogens.

We then sought to identify a putative specific signature of *M. humicola* infections. Despite considerable divergence in gene expression between N2 and JU2519 both before and after exposure to *M. humicola* (Data S2), we were able to find common genes responding to the pathogen (Figures S2A and S2B). These common genes showed a higher magnitude of change in the JU2519 background than in N2 (Figure S2A), likely reflecting a stronger infection in JU2519 in this experiment. Interestingly, within the common genes we found consistently members of a previously uncharacterised gene family, the *chitinase-like* (*chil*) gene family (Figure 3B and S2B). This family was a good candidate for a putative pathogen-specific response because *chil* gene induction was largely absent in differential gene expression datasets derived from infections by other pathogens (individual induced *chil* genes only appeared on average in 1.6 out of 42 gene sets– Data S3, see *chil_genes* tab– and as a group in 1 out of 212 microbe gene lists on WormExp [27]). The CHIL proteins contain a glycoside hydrolase family 18 domain (GH18), which is also found in catalytically active enzymes that hydrolyse glycosidic bonds, such as true chitinases. However, CHIL proteins lack the catalytic proton donor (Glu amino

acid in the motif DxxDxDxE), which is predicted to render them inactive [28–31]. Such non-catalytic proteins containing a GH18 domain are found in many organisms ranging from plants to invertebrates and mammals [32,33]. Although these genes have not been studied before in the context of oomycete infections, they have been linked to inflammation and immunity, for example against pathogenic nematodes, and there have been efforts to use them as disease biomarkers [34,35]. The *chil* gene family, the function of which was previously unknown, is expanded in *C. elegans* with 28 members annotated on Wormbase (Figure S2C). In contrast to *chil* genes, the expression of true chitinases was mostly unchanged in response to *M. humicola* exposure (Figure S2D).

We validated the induction of *chil* genes using quantitative RT-PCR (Figure S3A). To address the spatial distribution of expression, we constructed transgenic strains harbouring GFP fused to the promoter of either *chil-27* or *chil-28*, genes that were both reproducibly induced upon *M. humicola* infection. We found absence of GFP expression without exposure to the pathogen and inducible GFP activation upon exposure (Figures 3C and S3B). The GFP signal localised to the hypodermis since it co-localised with the constitutively expressed *col-12p::mCherry* transgene also used in the background as the co-injection marker (Figure S3C). We confirmed by single molecule FISH that *chil-27* mRNAs co-localise with GFP expressed from the *chil-27p::GFP* transgene, validating that the endogenous *chil-27* expression domain is the hypodermis (Figure 3D). Intriguingly, *chil-27* gene induction was graded from head to tail (Figure S3C), and even observed in animals exposed to autoclaved and thus inactivated pathogen (Figure 3C). Consistent with this, *chil-27* induction was found in animals exposed to active *M. humicola* that were neither showing symptoms of infection nor pathogen presence, as evidenced by the lack of pathogen detection with

FISH (Figures S3D and S3E). This indicates that *chil-27p::GFP* induction is likely to be a consequence of pathogen recognition as opposed to host damage caused by the infection.

To test whether the induction of *chil* genes is specific to *M. humicola* exposure, we subjected the strain carrying the *chil-27p::GFP* transcriptional reporter to biotic and abiotic stress. The biotic stress consisted of infection with various pathogens, such as a fungus (*D. coniospora*), bacterial species (*Microbacterium nematophilum*, *Serratia marcescens*) and microsporidia (*Nematocida parisii*, *Pancytospora epiphaga*) and therefore included pathogens that infect via distinct routes, either by entering through the mouth and later colonising the gut and epidermis, or penetrating directly through the cuticle. The abiotic stress included heat shock, ER stress, starvation, mechanical damage of the cuticle and osmotic shock. Interestingly, we found that none of the above treatments induced the *chil-27p::GFP* reporter (Figures S3F and S3G), highlighting the specificity of induction to *M. humicola* exposure.

We then tested whether the induction of *chil* genes modulates the sensitivity of *C. elegans* to oomycete infection. The majority of *chil* genes are clustered on two neighbouring locations on chromosome II, so we overexpressed them by using fosmids consisting of genomic fragments containing up to 9 *chil* gene family members at a time. We found that *chil* gene overexpression, as opposed to overexpression of an unrelated fosmid, resulted in reduced susceptibility to the infection whereas survival of these lines was not affected (Figures 4A, 4B and S4A-S4D). We next used CRISPR-Cas9 mediated genome editing to disrupt two consistently upregulated *chil* genes from each cluster by inserting a hygromycin resistance cassette within the coding region. In all cases, we found mild, yet

significant increase in sensitivity to infection with no major change in survival (Figures 4C, 4D, S4E and S4F). This is unlikely to be a consequence of the hygromycin resistance gene insertion because animals overexpressing this cassette did not display increased susceptibility to infection (Figure S4G). We conclude that the induction of CHIL proteins antagonises the infection by *M. humicola*.

We then investigated how *chil* gene induction might reduce susceptibility to *M. humicola* infections. As we did not find evidence for pathogen avoidance (Figures S4H and S4I), we reasoned that partial resistance might be linked to early events, such as reduced ability of the pathogen to attach to the cuticle and initiate the infection. To address this possibility, we devised attachment assays in which nematodes were left for 6 hours in proximity to the pathogen, followed by the quantification of attachment events using pathogen detection with FISH (Figure 4E). Interestingly, we found that animals overexpressing *chil* genes showed reduced pathogen attachment, and conversely, *chil* loss-of-function mutants exhibited increased pathogen attachment (Figure 4F). We hypothesised that these changes in pathogen attachment may be accompanied by broader changes in the composition of the cuticle that might influence its biomechanical properties. To address this possibility, we used atomic force microscopy (AFM) to generate force-displacement curves, whereby the displacement of the cuticle is measured upon delivering quantifiable forces [36]. Notably, we found that *chil* gene overexpression significantly changed the stiffness of the cuticle (Figures 4G, 4H, S4J and S4K). Instead, *chil* loss-of-function mutants did not show changes in stiffness, which is not surprising since these specific *chil* genes are mostly expressed upon exposure to the pathogen (Figure S4L). Taken together, we propose that *chil* gene induction may modify the properties of the cuticle in a way that prevents *M. humicola* attachment, thereby rendering the

pathogen unable to initiate an infection. This function might be indirect, as the majority of CHIL proteins do not contain a predicted signal peptide for secretion, thus they may not reach the cuticle and act instead intracellularly to modify some secreted component. Notably, recent evidence has also suggested a link between non-enzymatic chitinases and extracellular matrix formation modulating sensitivity of *Drosophila melanogaster* to bacterial infection [37]. Apart from the proposed role in cuticle modification, CHIL proteins may also act within the epidermis to regulate downstream signalling [38,39].

In summary, we present here a new pathosystem consisting of *C. elegans* as a host and its natural oomycete pathogen *M. humicola*. We anticipate that this new model will contribute to exploring oomycete infection strategies and molecular interactions with animal hosts. We demonstrate specificity in the *C. elegans* innate immunity response to *M. humicola* exposure and uncover downstream effectors that play a role to antagonise the infection. We also lay the groundwork for future studies that will be addressed towards dissecting the pathway involved in oomycete recognition and its link to the downstream innate immunity response. The paradigm of certain *chil* genes that are expressed at low levels during *C. elegans* culture in the lab but are induced to antagonise oomycete infections, highlights how gene functions can be revealed by studying model organisms in conditions closer to the wild environment [40].

Acknowledgements

We thank Iqrah Razzaq and Aurélien Richaud for technical help. We thank Sally Glockling, Gordon Beakes, Tolga Bozkurt and Lise Frézal for discussions. We thank Christopher Hammel, Rachel McMullan, Jonathan Ewbank for reagents and strains and Chris Spies for sharing unpublished data. Some strains were provided by the

CGC, which is funded by NIH Office of Research Infrastructure Programs (P40 OD010440). G.A.O was funded by a BBSRC DTP studentship. The Barkoulas lab is funded by the European Research Council (ROBUSTNET) and the Leverhulme Trust.

Author contributions

Conceptualization: G.A.O., M.K.F., S.L.K, M.B.; Investigation: G.A.O., M.K.F., S.L.K, K.K., C.L.E., M.A.S., G.Z., P.S., M-A.F. and M.B.; Writing: G.A.O., M.K.F., S.L.K, C.L.E., P.S., M-A.F. and M.B.; Supervision: M.B.; Funding Acquisition: M.B.

Declaration of Interests

The authors declare no competing interests

References

1. Félix, M.-A., and Braendle, C. (2010). The natural history of *Caenorhabditis elegans*. *Curr. Biol.* *20*, R965–R969.
2. Schulenburg, H., and Félix, M.A. (2017). The natural biotic environment of *Caenorhabditis elegans*. *Genetics* *206*, 55–86.
3. Kim, D.H., and Ewbank, J.J. (2015). Signaling in the innate immune response. *WormBook*, 1–51.
4. Irazoqui, J.E., Urbach, J.M., and Ausubel, F.M. (2010). Evolution of host innate defence: insights from *C. elegans* and primitive invertebrates. *Nat Rev Immunol* *10*, 47–58.
5. Irazoqui, J.E., Troemel, E.R., Feinbaum, R.L., Luhachack, L.G., Cezairliyan, B.O., and Ausubel, F.M. (2010). Distinct pathogenesis and host responses during infection of *C. elegans* by *P. aeruginosa* and *S. aureus*. *PLoS Pathog.* *6*, 1–24.
6. Wong, D., Bazopoulou, D., Pujol, N., Tavernarakis, N., and Ewbank, J.J.

- (2007). Genome-wide investigation reveals pathogen-specific and shared signatures in the response of *Caenorhabditis elegans* to infection. *Genome Biol.* *8*, R194.
7. Meisel, J.D., Panda, O., Mahanti, P., Schroeder, F.C., and Kim, D.H. (2014). Chemosensation of bacterial secondary metabolites modulates neuroendocrine signaling and behavior of *C. elegans*. *Cell* *159*, 267–280.
 8. Zugasti, O., Bose, N., Squiban, B., Belougne, J., Kurz, C.L., Schroeder, F.C., Pujol, N., and Ewbank, J.J. (2014). Activation of a G protein–coupled receptor by its endogenous ligand triggers the innate immune response of *Caenorhabditis elegans*. *Nat. Immunol.* *15*, 833–838.
 9. Beakes, G.W., Glockling, S.L., and Sekimoto, S. (2012). The evolutionary phylogeny of the oomycete “fungi.” *Protoplasma* *249*, 3–19.
 10. Bozkurt, T.O., Schornack, S., Banfield, M.J., and Kamoun, S. (2012). Oomycetes, effectors, and all that jazz. *Curr. Opin. Plant Biol.* *15*, 483–492.
 11. Raffaele, S., and Kamoun, S. (2012). Genome evolution in filamentous plant pathogens: Why bigger can be better. *Nat. Rev. Microbiol.* *10*, 417–430.
 12. Phillips, A.J., Anderson, V.L., Robertson, E.J., Secombes, C.J., and van West, P. (2008). New insights into animal pathogenic oomycetes. *Trends Microbiol.* *16*, 13–19.
 13. Barron, G.L., and Percy, J.G. (1975). Nematophagous fungi: a new Myzocytiium. *Can. J. Bot.* *53*, 1306–1309.
 14. Glockling, S.L., and Beakes, G.W. (2000). A review of the taxonomy, biology and infection strategies of “biflagellate holocarpic” parasites of nematodes. *Fungal Divers.* *4*, 1–20.
 15. Powell, J.R., and Ausubel, F.M. (2008). Models of *Caenorhabditis elegans*

- infection by bacterial and fungal pathogens. *Methods Mol. Biol.* 415, 403–427.
16. Kim, D.H., Feinbaum, R., Alloing, G., Emerson, F.E., Garsin, D.A., Inoue, H., Tanaka-Hino, M., Hisamoto, N., Matsumoto, K., Tan, M.-W., *et al.* (2002). A Conserved p38 MAP Kinase Pathway in *Caenorhabditis elegans* Innate Immunity. *Science* 297, 623–626.
 17. Troemel, E.R., Chu, S.W., Reinke, V., Lee, S.S., Ausubel, F.M., and Kim, D.H. (2006). p38 MAPK regulates expression of immune response genes and contributes to longevity in *C. elegans*. *PLoS Genet.* 2, e183.
 18. Pujol, N., Cypowyj, S., Ziegler, K., Millet, A., Astrain, A., Goncharov, A., Jin, Y., Chisholm, A.D., and Ewbank, J.J. (2008). Distinct Innate Immune Responses to Infection and Wounding in the *C. elegans* Epidermis. *Curr. Biol.* 18, 481–489.
 19. Cipollo, J.F., Awad, A.M., Costello, C.E., and Hirschberg, C.B. (2004). *srf-3*, a mutant of *Caenorhabditis elegans*, resistant to bacterial infection and to biofilm binding, is deficient in glycoconjugates. *J. Biol. Chem.* 279, 52893–903.
 20. Höflich, J., Berninsone, P., Göbel, C., Gravato-Nobre, M.J., Libby, B.J., Darby, C., Politz, S.M., Hodgkin, J., Hirschberg, C.B., and Baumeister, R. (2004). Loss of *srf-3*-encoded nucleotide sugar transporter activity in *Caenorhabditis elegans* alters surface antigenicity and prevents bacterial adherence. *J. Biol. Chem.* 279, 30440–30448.
 21. Bakowski, M.A., Desjardins, C.A., Smelkinson, M.G., Dunbar, T.A., Lopez-Moyado, I.F., Rifkin, S.A., Cuomo, C.A., and Troemel, E.R. (2014). Ubiquitin-Mediated Response to Microsporidia and Virus Infection in *C. elegans*. *PLoS Pathog.* 10, e1004200.
 22. Chen, K., Franz, C.J., Jiang, H., Jiang, Y., and Wang, D. (2017). An

- evolutionarily conserved transcriptional response to viral infection in *Caenorhabditis* nematodes. *BMC Genomics* *18*, 303.
23. Couillault, C., Pujol, N., Reboul, J., Sabatier, L., Guichou, J.F., Kohara, Y., and Ewbank, J.J. (2004). TLR-independent control of innate immunity in *Caenorhabditis elegans* by the TIR domain adaptor protein TIR-1, an ortholog of human SARM. *Nat. Immunol.* *5*, 488–494.
 24. Zugasti, O., and Ewbank, J.J. (2009). Neuroimmune regulation of antimicrobial peptide expression by a noncanonical TGF-beta signaling pathway in *Caenorhabditis elegans* epidermis. *Nat. Immunol.* *10*, 249–256.
 25. Sarkies, P., Ashe, A., Le Pen, J., McKie, M.A., and Miska, E.A. (2013). Competition between virus-derived and endogenous small RNAs regulates gene expression in *Caenorhabditis elegans*. *Genome Res.* *23*, 1258–70.
 26. Reddy, K.C., Dror, T., Sowa, J.N., Panek, J., Chen, K., Lim, E.S., Wang, D., and Troemel, E.R. (2017). An Intracellular Pathogen Response Pathway Promotes Proteostasis in *C. elegans*. *Curr. Biol.* *27*, 3544–3553.
 27. Yang, W., Dierking, K., and Schulenburg, H. (2015). WormExp: A web-based application for a *Caenorhabditis elegans*-specific gene expression enrichment analysis. *Bioinformatics* *32*, 943–945.
 28. Renkema, G.H., Boot, R.G., Au, F.L., Donker-koopman, W.E., and Strijland, A. (1998). Chitotriosidase, a chitinase, and the 39-kDa human cartilage glycoprotein, a chitin-binding lectin, are homologues of family 18 glycosyl hydrolases secreted by human macrophages. *Eur. J. Biochem* *251*, 504–509.
 29. Chang, N.C.A., Hung, S.I., Hwa, K.Y., Kato, I., Chen, J.E., Liu, C.H., and Chang, A.C. (2001). A Macrophage Protein, Ym1, Transiently Expressed during Inflammation Is a Novel Mammalian Lectin. *J. Biol. Chem.* *276*,

- 17497–17506.
30. Houston, D.R., Recklies, A.D., Krupa, J.C., and Van Aalten, D.M.F. (2003). Structure and ligand-induced conformational change of the 39-kDa glycoprotein from human articular chondrocytes. *J. Biol. Chem.* 278, 30206–30212.
 31. Zaheer-ul-Haq, Dalal, P., Aronson, N.N., and Madura, J.D. (2007). Family 18 chitolectins: Comparison of MGP40 and HUMGP39. *Biochem. Biophys. Res. Commun.* 359, 221–226.
 32. Funkhouser, J.D.J., and Aronson, N.N. (2007). Chitinase family GH18: evolutionary insights from the genomic history of a diverse protein family. *BMC Evol. Biol.* 7, 96.
 33. Bussink, A.P., Speijer, D., Aerts, J.M.F.G., and Boot, R.G. (2007). Evolution of mammalian chitinase(-like) members of family 18 glycosyl hydrolases. *Genetics* 177, 959–970.
 34. Kzhyshkowska, J., Gratchev, A., and Goerdt, S. (2007). Human Chitinases and Chitinase-Like Proteins as Indicators for Inflammation and Cancer. *Biomark. Insights* 2, 128–146.
 35. Sutherland, T.E., Logan, N., Ruckerl, D., Humbles, A.A., Allan, S.M., Papayannopoulos, V., Stockinger, B., Maizels, R.M., and Allen, J.E. (2014). Chitinase-like proteins promote IL-17-mediated neutrophilia in a tradeoff between nematode killing and host damage. *Nat. Immunol.* 15, 1116–1125.
 36. Essmann, C.L., Elmi, M., Shaw, M., Anand, G.M., Pawar, V.M., and Srinivasan, M.A. (2017). In-vivo high resolution AFM topographic imaging of *Caenorhabditis elegans* reveals previously unreported surface structures of cuticle mutants. *Nanomedicine Nanotechnology, Biol. Med.* 13, 183–189.

37. Pesch, Y., Riedel, D., Patil, K.R., Loch, G., and Behr, M. (2016). Chitinases and Imaginal disc growth factors organize the extracellular matrix formation at barrier tissues in insects. *Sci. Rep.* *6*, 18340.
38. Lee, C.G., Da Silva, C.A., Dela Cruz, C.S., Ahangari, F., Ma, B., Kang, M.-J., He, C.-H., Takyar, S., and Elias, J.A. (2011). Role of chitin and chitinase/chitinase-like proteins in inflammation, tissue remodeling, and injury. *Annu. Rev. Physiol.* *73*, 479–501.
39. Kucerova, L., Broz, V., Arefin, B., Maaroufi, H.O., Hurychova, J., Strnad, H., Zurovec, M., and Theopold, U. (2016). The *Drosophila* Chitinase-Like Protein IDGF3 Is Involved in Protection against Nematodes and in Wound Healing. *J. Innate Immun.* *8*, 199–210.
40. Petersen, C., Dirksen, P., and Schulenburg, H. (2015). Why we need more ecology for genetic models such as *C. elegans*. *Trends Genet.* *31*, 120–127.
41. Engelmann, I., Griffon, A., Tichit, L., Montañana-Sanchis, F., Wang, G., Reinke, V., Waterston, R.H., Hillier, L.W., and Ewbank, J.J. (2011). A Comprehensive Analysis of Gene Expression Changes Provoked by Bacterial and Fungal Infection in *C. elegans*. *PLoS One* *6*, e19055.
42. Brenner, S. (1974). The genetics of *Caenorhabditis elegans*. *Genetics* *77*, 71–94.
43. Levesque, C.A., and De Cock, A. (2004). Molecular phylogeny and taxonomy of the genus *Pythium*. *Mycol. Res.* *108*, 1363–1383.
44. Robideau, G.P., De Cock, A.W.A.M., Coffey, M.D., Voglmayr, H., Brouwer, H., Bala, K., Chitty, D.W., Désaulniers, N., Eggertson, Q.A., Gachon, C.M.M., *et al.* (2011). DNA barcoding of oomycetes with cytochrome c oxidase subunit I and internal transcribed spacer. *Mol. Ecol. Resour.* *11*, 1002–1011.

45. Spies, C.F.J., Grooters, A.M., Lévesque, C.A., Rintoul, T.L., Redhead, S.A., Glockling, S.L., Chen, C. yu, and de Cock, A.W.A.M. (2016). Molecular phylogeny and taxonomy of *Lagenidium*-like oomycetes pathogenic to mammals. *Fungal Biol.* *120*, 931–947.
46. Barkoulas, M., van Zon, J.S., Milloz, J., van Oudenaarden, A., and Félix, M.-A. (2013). Robustness and Epistasis in the *C. elegans* Vulval Signaling Network Revealed by Pathway Dosage Modulation. *Dev. Cell* *24*, 64–75.
47. Perales, R., King, D.M., Aguirre-Chen, C., and Hammell, C.M. (2014). LIN-42, the *Caenorhabditis elegans* PERIOD homolog, Negatively Regulates MicroRNA Transcription. *PLoS Genet.* *10*, e1004486
48. Langmead, B., and Salzberg, S.L. (2012). Fast gapped-read alignment with Bowtie 2. *Nat Methods* *9*, 357–359.
49. Quinlan, A.R., and Hall, I.M. (2010). BEDTools: A flexible suite of utilities for comparing genomic features. *Bioinformatics* *26*, 841–842.
50. Love, M.I., Huber, W., and Anders, S. (2014). Moderated estimation of fold change and dispersion for RNA-seq data with DESeq2. *Genome Biol.* *15*, 550.
51. Subramanian, A., Tamayo, P., Mootha, V.K., Mukherjee, S., and Ebert, B.L. (2005). Gene set enrichment analysis: A knowledge-based approach for interpreting genome-wide. *PNAS* *102*, 15545–15550.
52. Mootha, V.K., Lindgren, C.M., Eriksson, K., Subramanian, A., Sihag, S., Lehar, J., Puigserver, P., Carlsson, E., Ridderstråle, M., Laurila, E., *et al.* (2003). PGC-1 α -responsive genes involved in oxidative phosphorylation are coordinately downregulated in human diabetes. *Nat. Genet.* *34*, 267–273.
53. Chen, C., Fenk, L.A., and de Bono, M. (2013). Efficient genome editing in *Caenorhabditis elegans* by CRISPR-targeted homologous recombination.

- Nucleic Acids Res. *41*, e193–e193.
54. Friedland, A.E., Tzur, Y.B., Esvelt, K.M., Colaiácovo, M.P., Church, G.M., and Calarco, J. a (2013). Heritable genome editing in *C. elegans* via a CRISPR-Cas9 system. *Nat. Methods* *10*, 741–3.
 55. Pujol, N., Zugasti, O., Wong, D., Couillault, C., Kurz, C.L., Schulenburg, H., and Ewbank, J.J. (2008). Anti-fungal innate immunity in *C. elegans* is enhanced by evolutionary diversification of antimicrobial peptides. *PLoS Pathog.* *4*, e1000105
 56. Frøkjær-jensen, C., Davis, M.W., Ailion, M., and Jorgensen, E.M. (2012). Improved Mos1-mediated transgenesis in *C. elegans*. *Nat. Methods* *9*, 117–118.

Figure Legends

Figure 1. *M. humicola* is a new natural pathogen of *C. elegans*.

(A) *M. humicola* infected N2 animals exhibit ‘pearl’-like structures filling their entire body. (B-I) *M. humicola* stages during infection of *C. elegans*. Sporangia in infected animals initially contain undifferentiated cytoplasmic mass (B). After maturation, an exiting tube is formed (C) and zoospores are released (D, white arrows point to zoospores). The zoospores produce adhesive buds (E). Upon their attachment to the cuticle (F, white arrows), they penetrate inside (G) and non-septate hyphal growth is initiated (H, arrows point to the hypha). The hypha later partitions into distinct sporangia (I). (J-M) FISH staining of *M. humicola* growing in *C. elegans*. Red signal corresponds to a Cy5 probe targeting the pathogen 18S rRNA and L30 ribosomal subunit mRNA, blue is DAPI staining of *C. elegans* and pathogen nuclei. Pathogen can be visualized while entering the host (J), growing as hyphae (K) or forming

sporangia within the host (L). No Cy5 signal is observed in animals without exposure to the pathogen (M). **(N-O)** Scanning electron micrographs of infected versus non-infected *C. elegans* N2 animals. Note pathogen attachment along the alae (N) and mouth (O), n >100 animals analysed. Scale bar in J, K, N, O is 10 μm and in L, M is 100 μm . See also Figure S1 and Data S1.

Figure 2. Assessing *C. elegans* sensitivity to *M. humicola* infection.

(A) Cartoon depicting the infection assay devised to study the sensitivity of *C. elegans* to *M. humicola* infection. Note the arrangement of provided pathogen within the OP50 lawn. **(B)** Comparison of infection assays using synchronised N2 animals performed at 25°C and 20°C. Note increase in sensitivity at 25°C (log-rank p value < 0.0001) **(C-D)** Infection (C) and survival (D) assays for the p38 MAPK pathway mutants *pmk-1(km25)* and *sek-1(km4)* compared to N2. Note that both mutants show increased sensitivity to *M. humicola* ($p < 0.0001$). **(E-F)** Infection (E) and survival (F) assays for *srf-3(e2689)* mutants in comparison to N2. Note an increase in sensitivity to infection in the mutant background ($p < 0.0001$). The data shown here are representative of at least three independent experiments and experiments were done in triplicates with n = 50 synchronised animals per assay. See also Figure S1.

Figure 3. *chil* genes are induced in the hypodermis upon exposure to *M. humicola*.

(A) Venn diagrams of genes differentially expressed at 12 hours post exposure to *D. coniospora* in N2, and 12 / 24 hours (pooled data) post exposure to *M. humicola* in N2 (left) or JU2519 (right). *M. humicola* data are from Data S2 and *D. coniospora* data from [41]. **(B)** Heat map showing the expression of *chil* genes in N2 and JU2519

12 and 24 hours post exposure to *M. humicola*. **(C)** Induction of GFP signal in *chil-27p::GFP* transgenic animals following exposure to live *M. humicola* or inactivated (autoclaved) *M. humicola*. No *chil-27p::GFP* expression was observed in the absence of pathogen. Note that the *col-12p::mCherry* transgene is constitutively expressed in the hypodermis. All panels show aligned *C. elegans* animals arranged together in a cluster, n >100 animals in all cases. **(D)** *chil-27* expression detected by smFISH in a strain carrying the *chil-27p::GFP* reporter post exposure to *M. humicola*. White spots correspond to *chil-27* mRNAs and co-localise with GFP labelled nuclei. No *chil-27* expression was observed without exposure to *M. humicola*. Scale bars in C and D are 100 and 10 μm respectively. See also Figure S2, Figure S3, Data S2 and Data S3.

Figure 4. *chil* genes antagonise *C. elegans* infection by *M. humicola*.

(A-B) Transgenic animals carrying fosmid containing *chil* genes 1-9 (A) or 18-27 (B) display significantly decreased susceptibility to *M. humicola* infection in comparison to N2. **(C-D)** Mutations in *chil-4*, *chil-9* (C), *chil-18*, *chil-27* (D) increases host susceptibility to *M. humicola* infection in comparison to N2. **(E)** Cartoon depicting the assay used to quantify pathogen attachment events on the host cuticle. Pathogen is detected with FISH as in Figure 1. Images show close-ups of a single animal with pathogen attachment (bright spots) as opposed to an animal without attachment. **(F)** Quantification of pathogen attachment in transgenic animals carrying fosmid containing *chil* genes 1-9 or 18-27 and mutations in *chil-4*, *chil-9*, *chil-18* or *chil-27*. Data are shown as mean frequency \pm standard error of the proportion, n>100 animals per genotype. **(G-H)** Force-displacement curves using AFM. Transgenic animals carrying fosmid containing *chil* genes 1-9 (G) or 18-27 (H) show reduction in stiffness, n>20 animals per genotype, 2 quantifications per

animal. Stars in A-D and F show statistically significant changes with a log-rank test (A-D) or chi-squared test (F) as follows: * $p < 0.05$, ** $p < 0.01$, *** $p < 0.001$, **** $p < 0.0001$. The data shown for panels A-D are representative of at least three independent experiments, all conducted in triplicates. See also Figure S4.

STAR Methods

Contact for Reagent and Resource Sharing

Further information and requests for reagents should be directed to and will be fulfilled by the Lead Contact, Michalis Barkoulas (m.barkoulas@imperial.ac.uk).

Experimental Model and Subject Details

Nematode and pathogen culture

C. elegans and other nematodes were cultured on NGM plates seeded with *E. coli* OP50 and maintained at 20°C under standard conditions [42]. The *C. elegans* Bristol isolate (N2) was used as the lab wild-type reference strain. JU2519 was sampled from rotten figs (*Ficus isophlebia*) in the botanical garden of Lisbon, Portugal on 25 Aug 2013 and it was the wild isolate naturally carrying the pathogen *M. humicola*. The infection started from a single isolated dauer larva that was carrying the pathogen. The pathogen was maintained on NGM plates containing *C. elegans* at 25°C and chunked every two or three days, occasionally adding fresh nematodes to the pathogen culture. The infection spreads horizontally within the population and can be cured by bleaching the nematode culture (standard *C. elegans* technique to isolate eggs that are resistant to bleach due to the impermeable egg shell). Molecular characterisation (see Data S1) was carried out by using universal eukaryotic primers UN-up18S42 and UN-1o28S22 to amplify internal transcribed spacer 1 and 2, Myzo18S/18AS oligos to amplify the 18S rDNA and Cox2F/Cox-2R oligos to amplify the cytochrome c oxidase subunit 2 gene [43–45]. The complete list of strains used in this study can be found in the Key Resources Table and a list of primers in Table S1.

Method Details

Infection, attachment and avoidance assays

All infection assays were carried out at 25°C on NGM plates seeded with 50 µl lawns of OP50 using synchronized L4 animals. Infection assays were carried out in triplicates and consisted of 50 animals being transferred onto plates containing OP50 and 3 infected animals (placed in a triangle as shown in Figure 2A), or onto control OP50 plates devoid of pathogen. Animals were exposed to the pathogen for the first 48 hours and transferred every 24 hours to new plates for the remainder of the assay. Plates were scored every 24 hours over a period of 6-7 days for the number of infected (defined as nematodes containing visible sporangia). Dead (unresponsive to touch yet not developing visible sporangia) or missing animals were censored. As a control for the infection assays, the same population of tested animals was also maintained simultaneously on NGM plates, but devoid of the pathogen, and the number of dead animals was monitored, whilst the number of missing animals was censored. Experiments were reproduced at least three times and GraphPad Prism 7 (GraphPad Software Inc.) was used to plot and compare survival curves. The log-rank test was used to assess statistical significance and a p value of <0.05 was considered significant.

To perform attachment assays, 100 L4 animals were placed into 24-well plates containing NGM seeded with OP50 together with 10 infected animals. The plates were incubated for 6 hours at 25°C and then the animals were washed off using M9. The animals were immediately fixed and processed for FISH as previously described [46] using Cy5-labelled oligos targeting the 18S rRNA and L30 ribosomal subunit mRNA of *M. humicola* (Table S1). Animals were imaged on slides using a Zeiss Axio Zoom V16 (Zeiss) equipped with an Axio 506 mono camera. Animals were scored as

positive or negative for attachment based on the presence of bright fluorescent spots along the cuticle that correspond to pathogen attachment sites.

To test for a putative host behaviour to avoid *M. humicola*, two different protocols were used. First, 20 day-1 adults were added to small OP50 lawns on 90 mm NGM plates with (3 dead infected animals) or without pathogen. After 4, 10 and 24 hours, the percentage of animals avoiding the OP50 lawns was scored. In the second protocol, 20 day-1 adults were added to the centre of 90 mm NGM plates with two small OP50 lawns with (3 dead infected animals) or without pathogen. After 4, 10 and 24 hours, the percentage of animals on each of the two lawns was scored. All behaviour assays were performed in triplicates.

Molecular cloning and transgenesis

The transcriptional reporter *chil-27p::GFP* transgene was generated by amplifying a 1.6 kb genomic fragment containing sequences upstream of the *chil-27* start codon using primers pchil-27F and pchil-27R. The amplicon was cloned into the vector L3135 as a HindIII / XbaI fragment, resulting in plasmid pGO4. The transcriptional reporter construct *chil-28p::GFP* was produced in a similar manner by amplifying a 0.4kb fragment using primers pchil-28F/R respectively, thus producing construct pGO7. These constructs were injected into N2 at a concentration of 30 ng/μl together with 20 ng/μl of plasmid pCMH1195 [*col-12p::mCherry-pest*] as a co-injection marker [47]. Extrachromosomal arrays were integrated in the genome via standard gamma irradiation.

To produce *chil-1* to *chil-9* and *chil-18* to *chil-27* (excluding *chil-24* which is located elsewhere in the genome) overexpression lines, we injected into N2 fosmid clones WRM065aH01 and WRM0619bB10 (Source Bioscience) respectively. Note

that each of these fosmids also contains 4 other genes. Fosmids were injected at a concentration of 20 ng/μl with 5ng/μl of *myo-2p::GFP* as a co-injection marker. In each instance, three independent lines were obtained and used for analysis. Control lines were created by injecting fosmid WRM0627dG07 at 50 ng/μl and the hygromycin resistance cassette at 10 ng/μl together with *myo-2p::GFP* at 5 ng/μl.

RNAseq analysis

Infection and control assays were set up in triplicates as described above, and RNA was extracted at 12 and 24 hours post exposure to the pathogen from a total of 50 animals per plate using the TRIzol reagent and the Direct-zol RNA extraction kit (Zymo Research) according to the manufacturer's instructions. The quality and quantity of RNA was determined using the Agilent RNA ScreenType System on an Agilent 2100 Bioanalyzer. The Illumina TruSeq stranded RNA library preparation kit was used for library preparation. The sequencing data were processed and aligned to *C. elegans* reference transcriptome using Bowtie2 [48]. The alignments were converted to counts using bedtools [49]. The counts were then normalised using DESeq2 package in R 3.3.2 [50]. The differences in gene expression were calculated using the negative binomial test with Benjamini-Hochberg multiple test correction using DESeq2.

GSEA analysis

Our RNA-seq data were compared to other *C. elegans* transcriptomic datasets using Gene Set Enrichment Analysis (GSEA) software v2.0 [51,52]. The genes that were significantly differentially expressed upon infection (FDR<0.1) were ranked based on their log2fold change in descending order. We used for the analysis the gene sets compiled by [21] and added *E. faecalis*, *S. marcescens* and *P. luminescens* from [41]

and *B. thuringiensis* from WormExp [27]. GSEA was run in cases where there was an overlap of greater than 5 genes. Pre-ranked analysis with 1000 permutations for each analysis was performed independently for N2, JU2519 strains and the common genes between the two isolates at the 12 hours and 24 hours timepoint. The NES-values of gene sets with FDR<0.25 and nominal *p* value<0.05 were considered as significant and the results are summarized in Data S3.

CRISPR-mediated genome editing

To generate the *chil-4*, *9*, *8* and *27* CRISPR-mediated knock-outs we inserted a hygromycin resistance cassette [*rps-0p::hygB::unc54 3'UTR*] within the corresponding *chil* gene as previously described [53]. To this end, sgRNA constructs were generated as described in [54] to target the following *chil* gene sequences upstream of the PAM motif (*chil-4_GAAAGTAATGATCAGTATAGG*, *chil-9_GAAAGTAATGATCAGCATAGG*, *chil-18_ATCTGCACCGTTGTATGG* and *chil-27_ACCTCTCAATATTCAAGTGG*). The repair templates for homologous recombination were constructed in a two-step method. Initially, we PCR amplified 0.8kb to 1kb of genomic region upstream (*chil-n_frg1* F/R oligos) and downstream (*chil-n_frg2* F/R oligos) of the PAM motif and the HygR cassette (*hygro* F/R) and the resulting amplicons were assembled in a multi-fragment Gibson reaction using SpeI digested BJ97 as the backbone. The injection mix contained *eft3p::cas9* at 50ng/μl, *pU6::[respective chil gene sgRNA]* at 30 ng/μl, heat shock inducible toxin plasmid pMA122 [*hsp-16.41p:peel-1:tbb-2 3' UTR*] 10ng/μl, repair plasmid templates at 30ng/μl and *myo-2p::dsRed* at 5 ng/μl. PCR validations of the *chil* gene modifications were performed using chromosomal primers that anneal beyond the repair template together with an oligo that anneals within the hygromycin gene (*chil-27_F/chil-*

27_HygR, chil-18_HygF/R, chil-9_HygF/R, chil-4_HygF/R) and HygB gene specific primers (hygro-geno F/R).

Microscopy

To perform scanning electron microscopy, mixed-stage populations were collected from plates containing the pathogen, washed twice with M9 and fixed for 3 hours at room temperature in a solution containing 3% glutaraldehyde (Sigma) in M9. Fixed animals were then washed twice in M9 and dehydrated gradually from 15% to 100% ethanol. Samples were dried in a critical point dryer (K850, ProSciTech) and coated with gold/palladium for 2 x 90 seconds using the SC7620 Mini Sputter Coater (Quorum technologies). The samples were imaged in a JEOL JSM-6390 scanning electron microscope using 5 to 25 kVolt acceleration voltage.

For smFISH/FISH experiments, mixed-stage populations were fixed and processed as previously described [46]. Image acquisition was performed using an epifluorescence Ti-eclipse (Nikon) microscope equipped with a low noise CCD camera (Andor iKon-M934) and images were analysed using ImageJ.

To perform AFM, animals were prepared as described before [36]. Briefly, young adult animals were paralysed in 10 mg/ml 2,3-butanedione monoxime (Sigma) for 1 hour at room temperature and transferred to a ~2 mm thick 4% agarose bed in a petri dish (30 mm). Heads and tails were fixed with tissue glue (Dermabond, Ethicon) and the dish filled with 2.5 ml M9 buffer. AFM data were obtained using the NanoWizard3 (JPK) under aqueous conditions. Type NSC12 tipless cantilever with a 10 μm borosilicate bead (7.5 N/m; MikroMash) attached were used in force spectroscopy mode to obtain force-indentation measures at 450/400 nN force setpoint and 0.5 $\mu\text{m/s}$ indentation speed. Cantilever sensitivity and stiffness (k) were calibrated

using the JPK system calibration mode before each experiment. In all cases, we performed two independent AFM measurements per animal.

chil-27p::GFP reporter specificity

All *chil-27p::GFP* reporter induction assays were monitored using a Zeiss Axio Zoom V16 (Zeiss) over a period of 48 hours. Single infected animals were picked into an eppendorf tube, autoclaved at 121°C for 20 mins and then put back on an OP50 plate containing animals carrying the reporter. Heat shock was performed by placing L4 animals at 33°C for 4 hours or at 37°C for 1 hour. Mechanical damage involved piercing three times the cuticle of L4 animals immobilised in halocarbon *oil* (Sigma) with an injection needle. The starvation treatment was performed by placing L4 animals on NGM plates with ampicillin and without OP50 for 48 hours at 20°C. Hyperosmotic stress was induced by incubating L4 animals for 6h in a solution containing 300mM NaCl or on NGM plates supplemented with 300mM NaCl as in previous studies [55]. ER stress was induced by adding 0.5 µg/ml tunicamycin (Sigma) to NGM plates. Infections with bacteria and fungi were performed by moving L4 animals to NGM plates containing OP50 lawns together with *M. nematophilum*, *S. marcescens* or spores of *D. coniospora* in three replicates per experiment. For infections with microsporidia, 2 million spores were used to infect 20 L4s at 23°C and infection symptoms were verified by DIC microscopy. Note that *chil-27* gene induction has been reported at 24 hours post exposure to *Enterococcus faecalis* using Tiling arrays [41].

RT-qPCR

Total RNA was extracted from animals grown at 25 °C at the appropriate stage/exposure time using TRIzol followed by DNase treatment and isopropanol/ethanol precipitation. Quality and concentration were assessed using a NanoDrop Lite (Thermo Scientific) and gel electrophoresis. Superscript III (Invitrogen) with Oligo(dT)₁₅ (Promega) was used for cDNA synthesis according to the manufacturer's instructions. Real-time PCR was performed using LightCycler480 SYBR Green I Master (Roche) in a LightCycler480 instrument and analysed with the LightCycler480 software (absolute quantification analysis using second derivative maximum method). Ct values were normalized to the reference gene *pmp-3*. Experiments were performed in biological triplicates and all oligos are listed in Table S1.

Quantification and Statistical Analysis

All statistical details (statistical test used, number of samples, and *p* values) for each experiment can be found in the text and in the Figure legends. Graphic representation and statistical analyses were performed using the GraphPad Prism 7 software. Data shown in graphs indicate mean, and error bars represent standard error of the mean or proportion unless otherwise indicated. For infection assays, only dead animals with clear signs of infection were scored and all other dead or lost animals were censored. For respective control assays without pathogen, dead animals (unresponsive to touch) were scored and only lost animals were censored. A log-rank test, chi-squared test (F) or t-test was used to analyse data as described in Figure legends and data were considered statistically significant when $p < 0.05$. Asterisks in figures indicate corresponding statistical significance as defined (* $p < 0.05$; ** $p < 0.01$; *** $p < 0.001$; **** $p < 0.0001$).

The RNA-seq dataset we generated consists of 24 samples in total (N2_control_12 hours (3 replicates), N2_control_24 hours (3 replicates), JU2519_control_12 hours (3 replicates), JU2519_control_24 hours (3 replicates), N2_infected_12 hours (3 replicates), N2_infected_24 hours (3 replicates), JU2519_infected_12 hours (3 replicates), JU2519_infected_24 hours (3 replicates)). For the RNAseq analysis the differences in gene expression were calculated using the negative binomial test with Benjamini-Hochberg multiple test correction using DESeq2. For the GSEA analysis, the genes that were significantly differentially expressed upon infection (FDR<0.1) were ranked from most upregulated to most downregulated. The NES-values of gene sets with FDR<0.25 and nominal p-value<0.05 were considered as significant.

Data and Software availability

The raw data from the RNA-seq experiments have been deposited to NCBI GEO under accession GSE101647.

Supplemental item titles

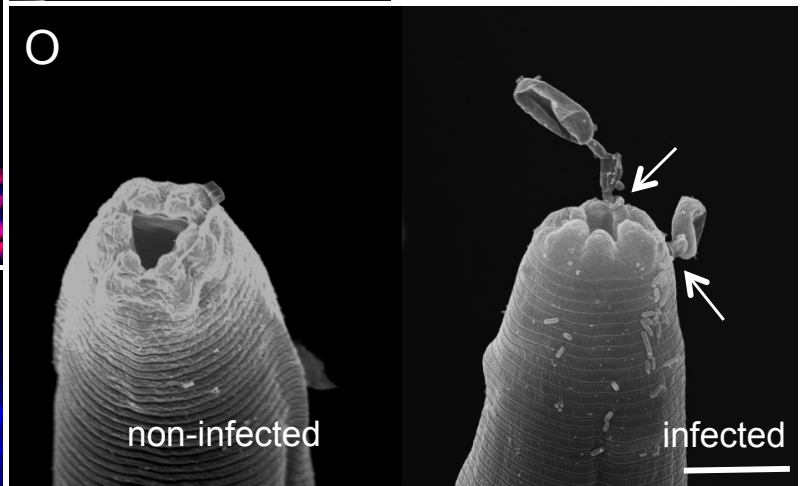
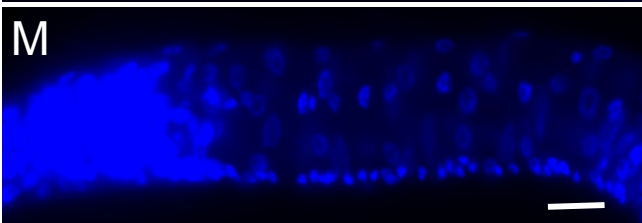
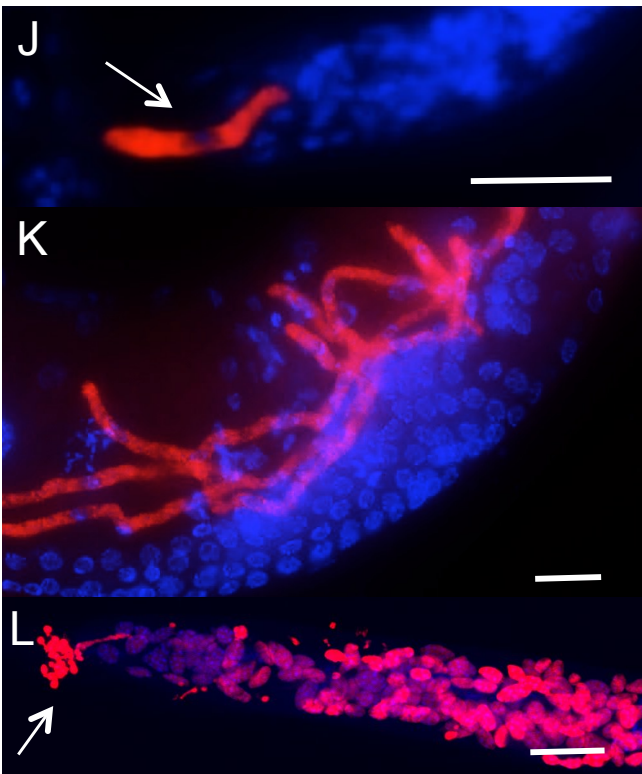
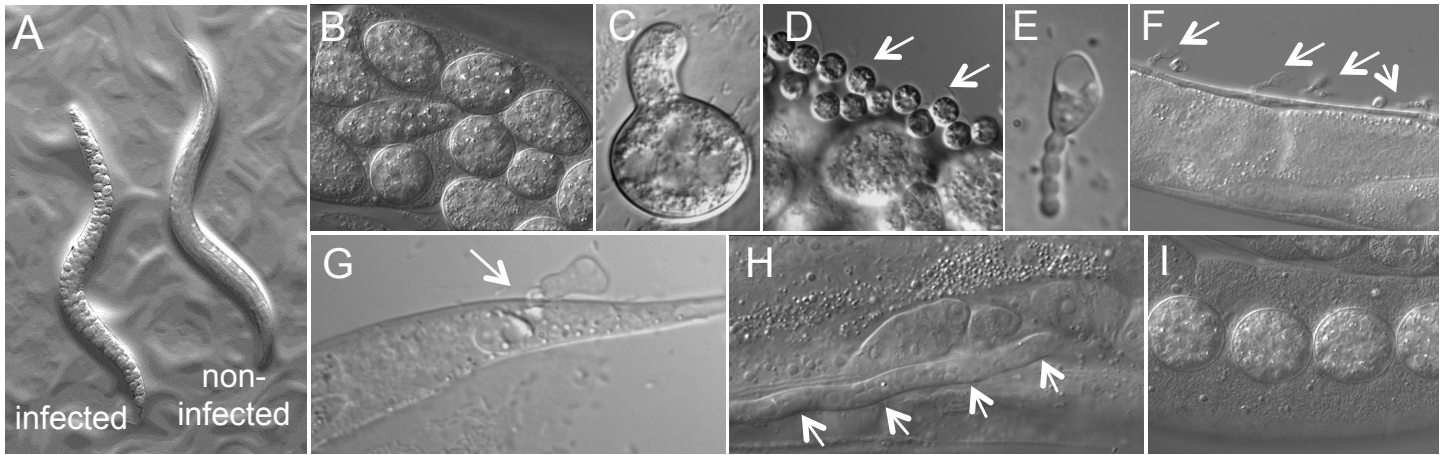
Table S1: List of oligos used in this study, related to STAR Methods.

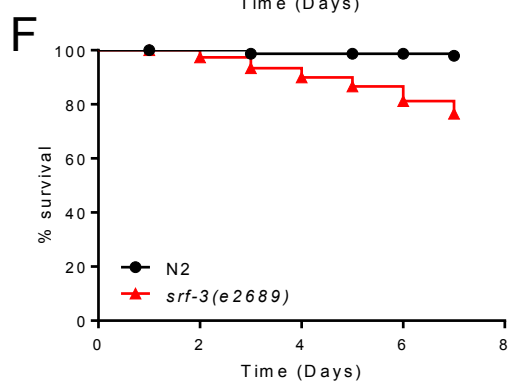
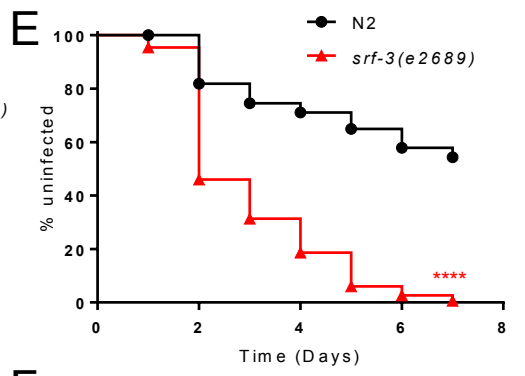
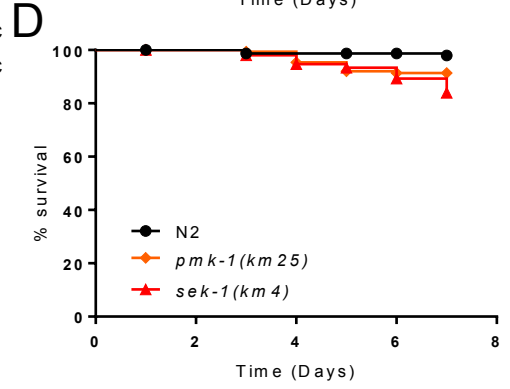
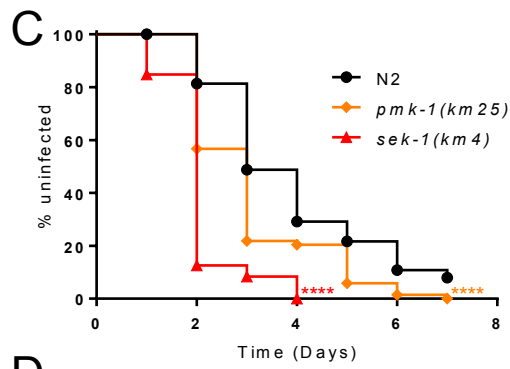
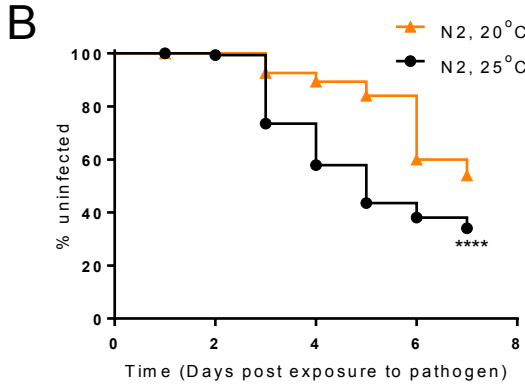
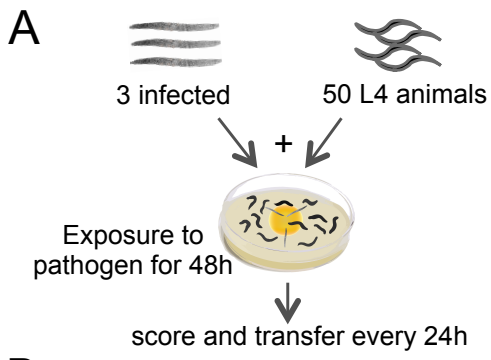
Data S1: Pairwise comparisons of percentage of similarity in *cox2*, ITS and 18S sequences between the Lisbon isolate and other *Myzocytiopsis* species, related to Figure 1 and STAR Methods.

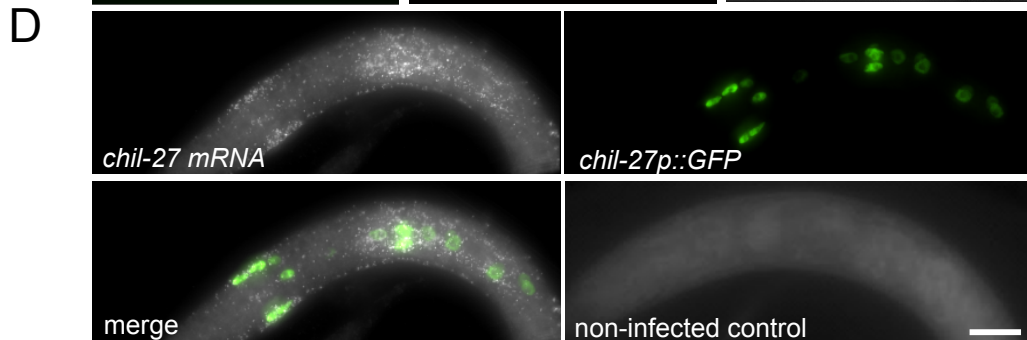
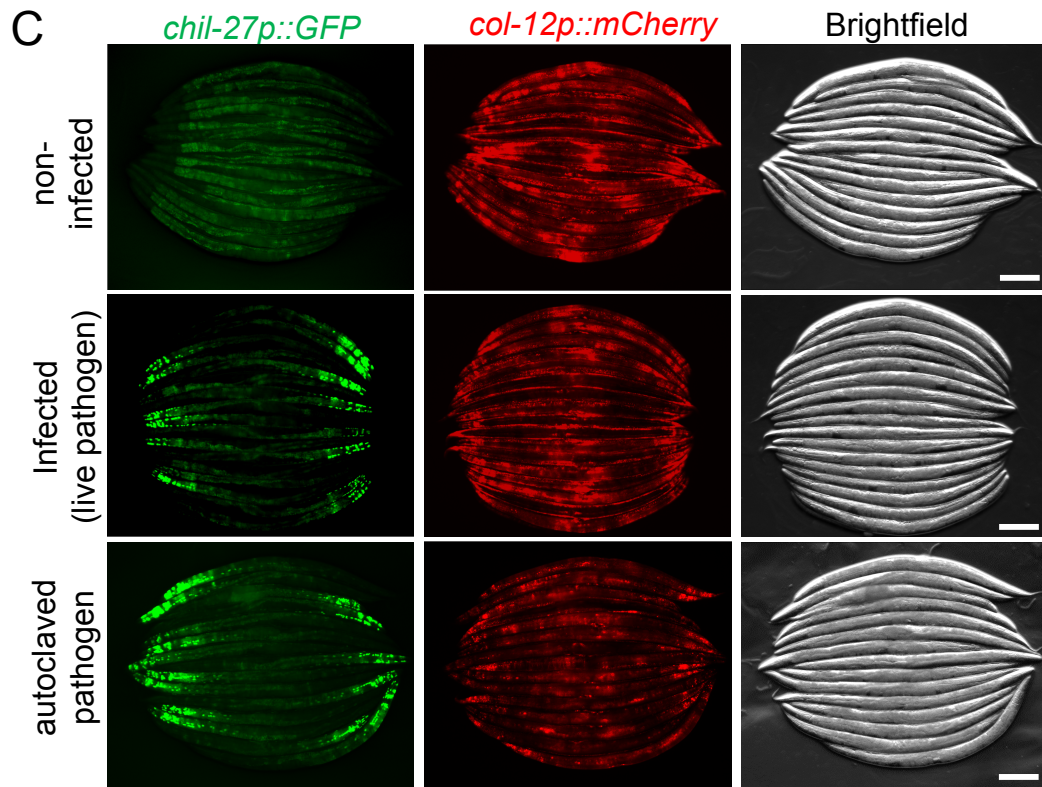
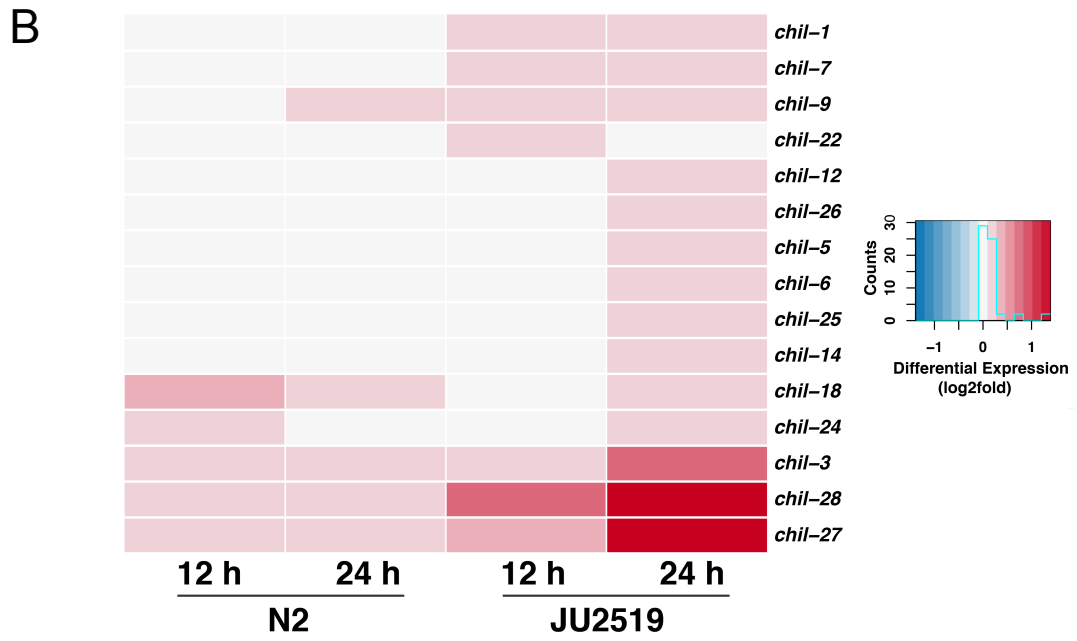
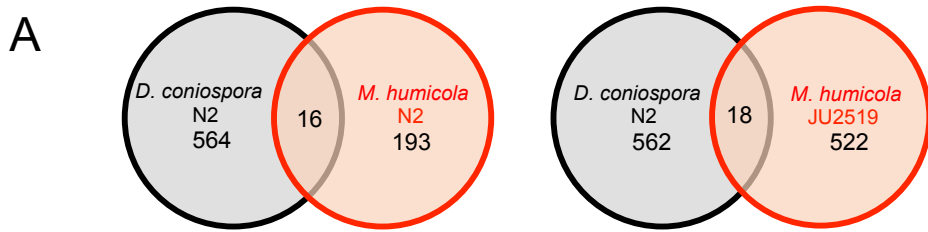
Data S2: Differential expression of genes as determined by DESeq2, related to Figure 3. This spreadsheet contains the following 10 tabs: (1-4) differential expression of genes in N2 and JU2519 at 12 hours and 24 hours post exposure to *M. humicola* (N2_12h / N2_24h, JU_12h / JU_24h), (5-8) differential expression of genes between N2 and JU2519 before (N2Con_JUCon_12h / N2Con_JUCon_24h)

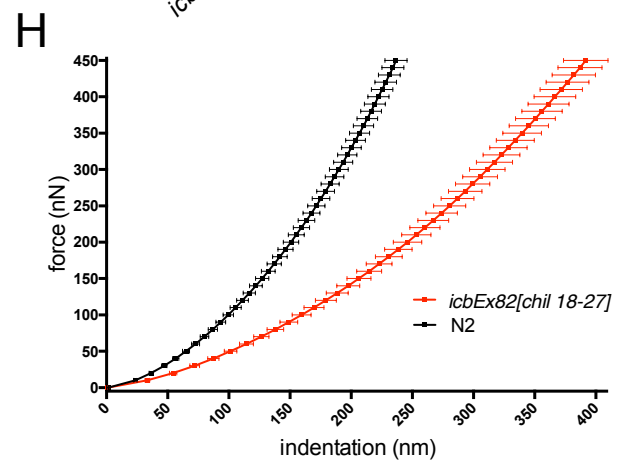
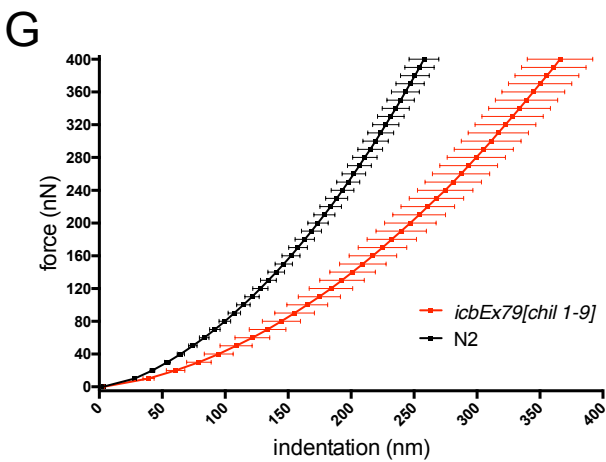
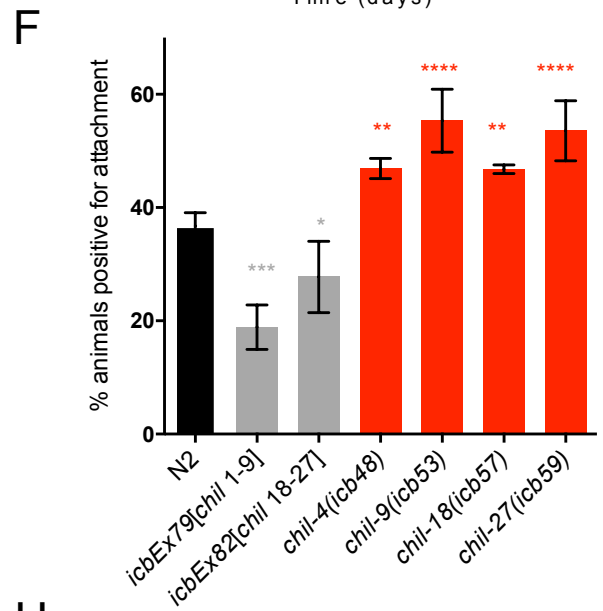
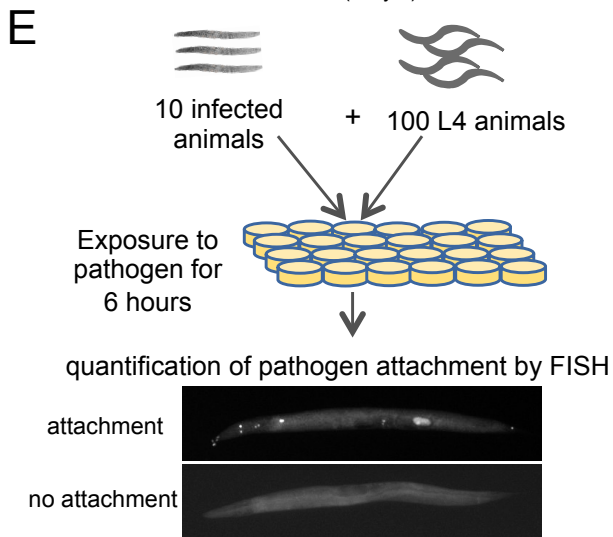
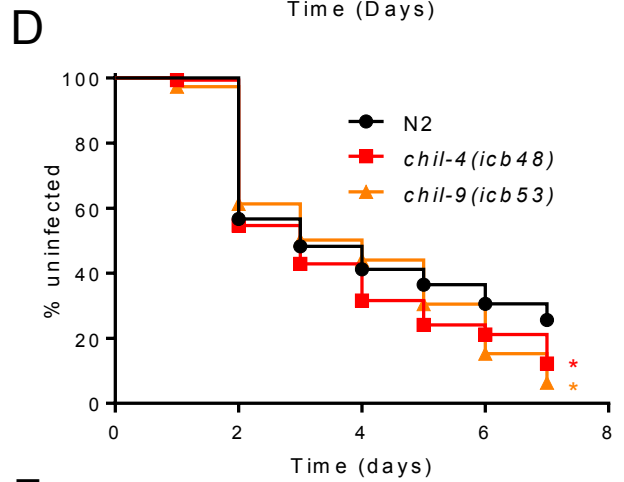
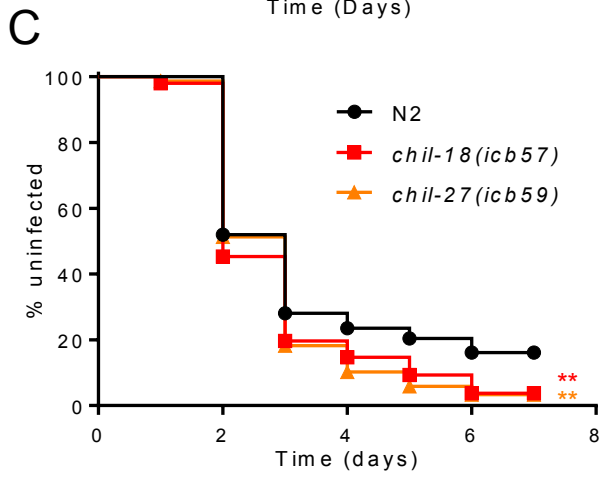
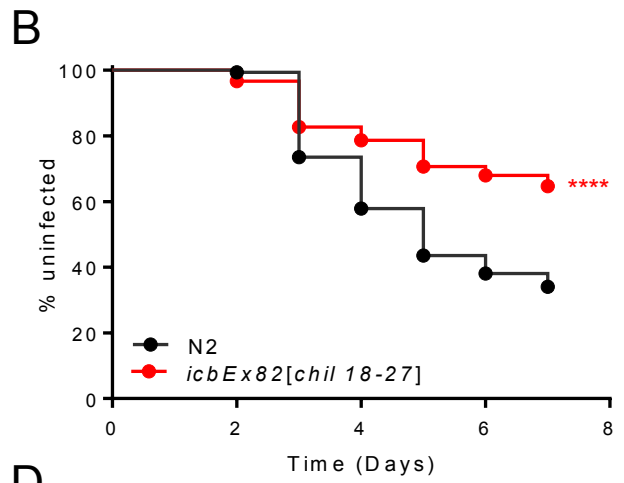
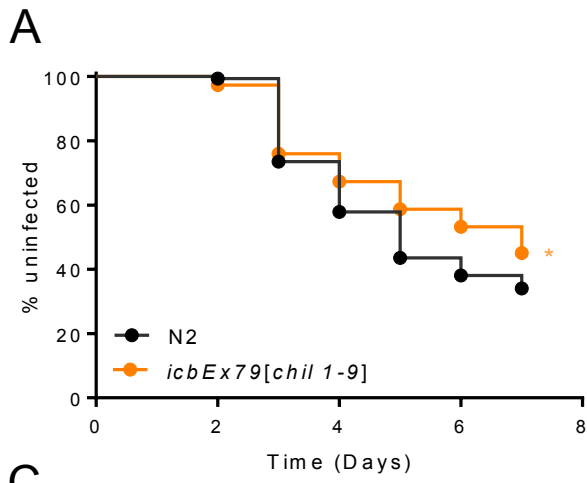
and after exposure to *Myzocytiopsis humicola* (N2Inf_JUInf_12h / N2Inf_JUInf_24h) and (9-10) common analysis for genes differentially expressed at 12 hours and 24 hours post exposure.

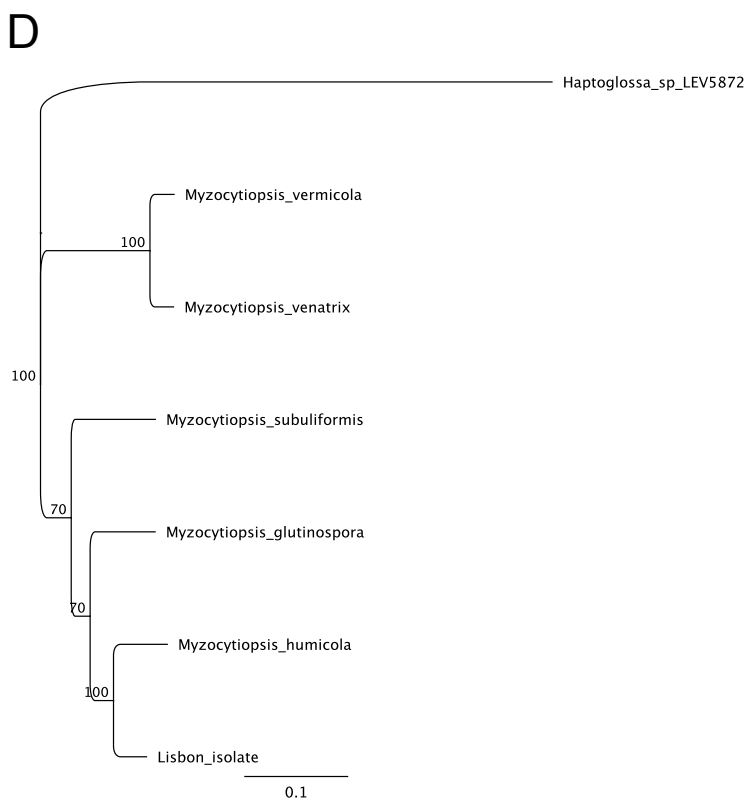
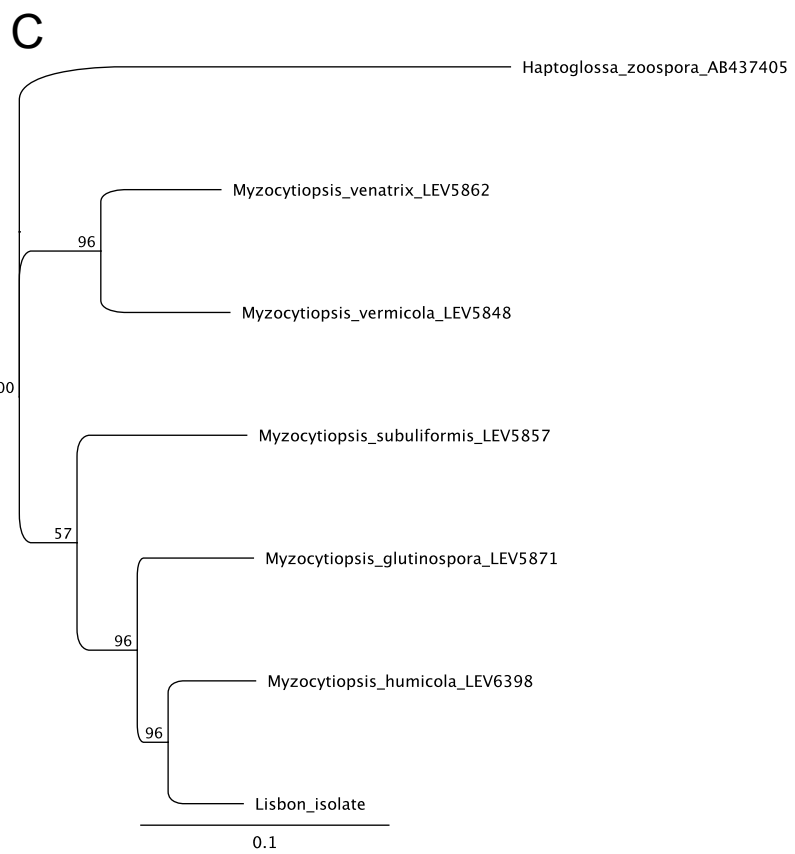
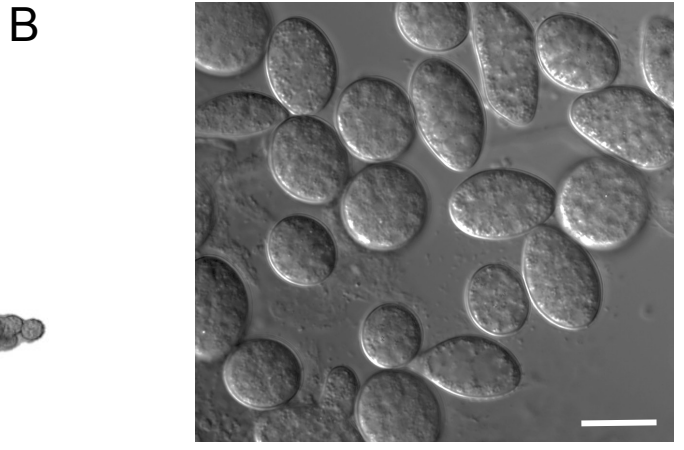
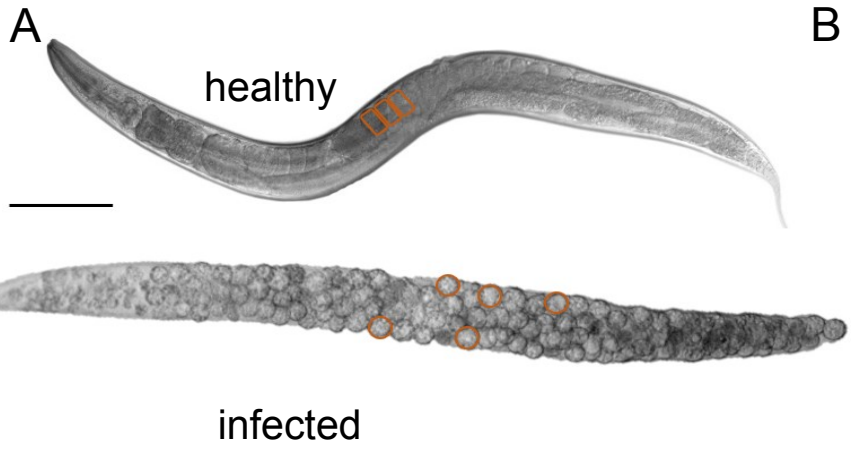
Data S3: Overlap between genes upregulated upon exposure to *M. humicola* and differentially expressed in infections by other pathogens, related to Figure 3 and STAR Methods. This spreadsheet contains 5 tabs: (1) The overlap tab shows the gene list sources used in our analysis and how many differentially expressed genes are in common between these gene sets and our *M. humicola* data set. For gene sets containing > 10 genes, overlap > 10% is highlighted in orange. (2) The GSEA tab shows the results of the gene set enrichment analysis. Significant intersection is highlighted in orange (NOM p-value < 0.05 and FDR < 0.25). Size refers to the number of common genes between the two datasets in question. (3-4) The genes GSEA tabs show the identity of common genes for cases where the GSEA identified significant intersection and how often these genes appear in all other 42 gene sets. Note that significant intersection was only found in JU2519 (genes GSEA JU2519_12h, genes GSEA JU2519_24h) and not in N2. (5) The *chil*_genes tab shows a quantification of how often the *M. humicola*-induced *chil* genes appear in other gene sets.











E

strain / species	N2	JU2519	JU2007	CB4856	JU1896	AF16	HK104	JU1886	PB4641	JU1184	RGD1	CEW1	PS312
	<i>C. elegans</i>	<i>C. elegans</i>	<i>C. elegans</i>	<i>C. elegans</i>	<i>C. elegans</i>	<i>C. briggsae</i>	<i>C. briggsae</i>	<i>C. brenneri</i>	<i>C. remanei</i>	<i>C. remanei</i>	<i>C. angaria</i>	<i>O. tipulae</i>	<i>P. pacificus</i>
<i>M. humicola</i> infection													

= susceptible

= non susceptible

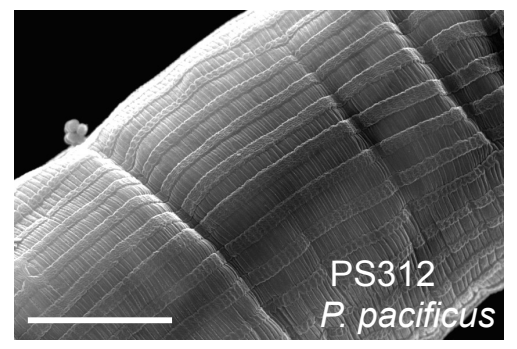
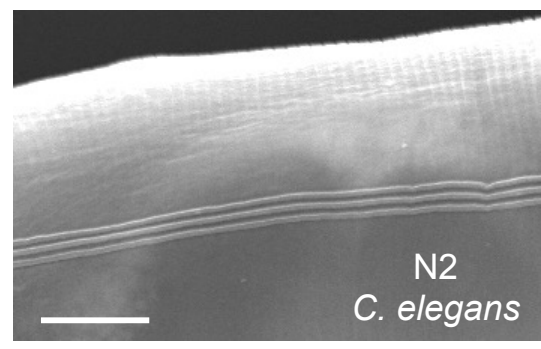


Figure S1. Characterisation of the new pathogen and its host specificity, related to Figure 1 and Figure 2.

(A) Infected animals develop sporangia throughout the body of the nematode (marked by orange circles). Healthy animals show no sporangia and contain eggs instead (marked by orange rectangles). (B) Close-up of sporangia released on a petri dish. (C-D) Phylogenetic trees showing the genetic similarity between the Lisbon isolate and *M. humicola* based on *cox2* (C) and ITS (D) sequences. The neighbour-joining consensus tree was created with Geneious version 9.1.5. A basal oomycete (*Haptoglossa*) was used as an outgroup. The numbers at the branch nodes indicate bootstrap values based on 100 replicates, labels with less than 50% support are not shown. (E) Qualitative assessment of host specificity of *M. humicola* infections. *P. pacificus* strain PS312 was found to be insensitive to *M. humicola* using the standard infection assay Ttshown in Figure 2A. The experiment has been repeated three times, n> 150 animals. Note that cuticle morphology in *P. pacificus* is different to N2, as shown by the SEM images. Scale bars are 150 μm in A, 20 μm in B and 10 μm in E.

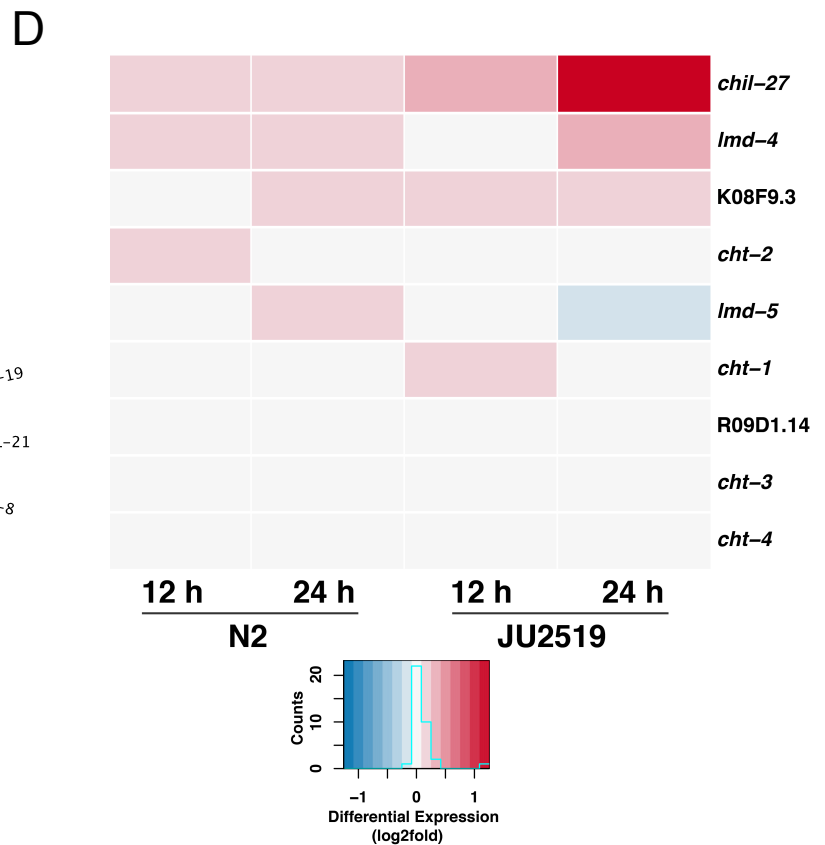
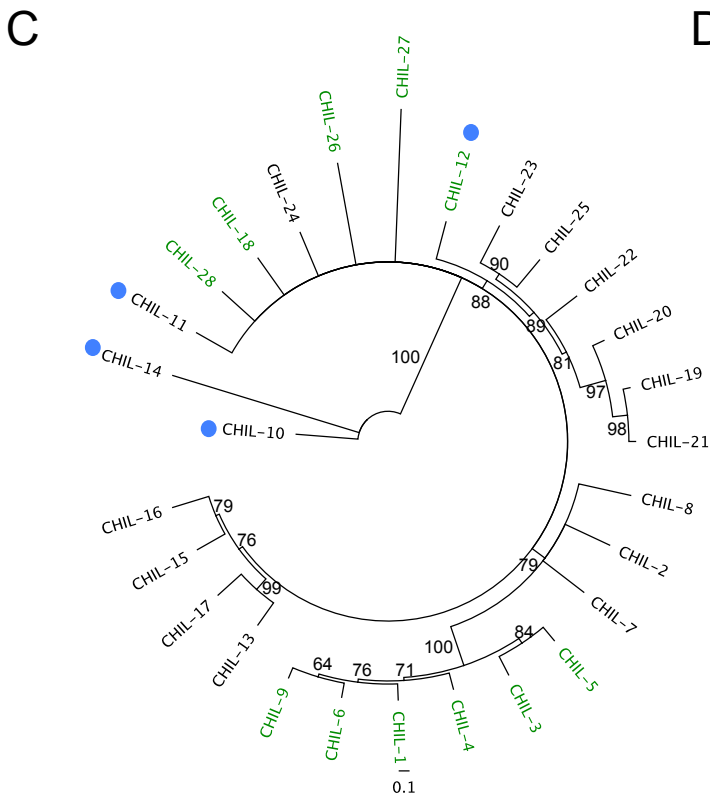
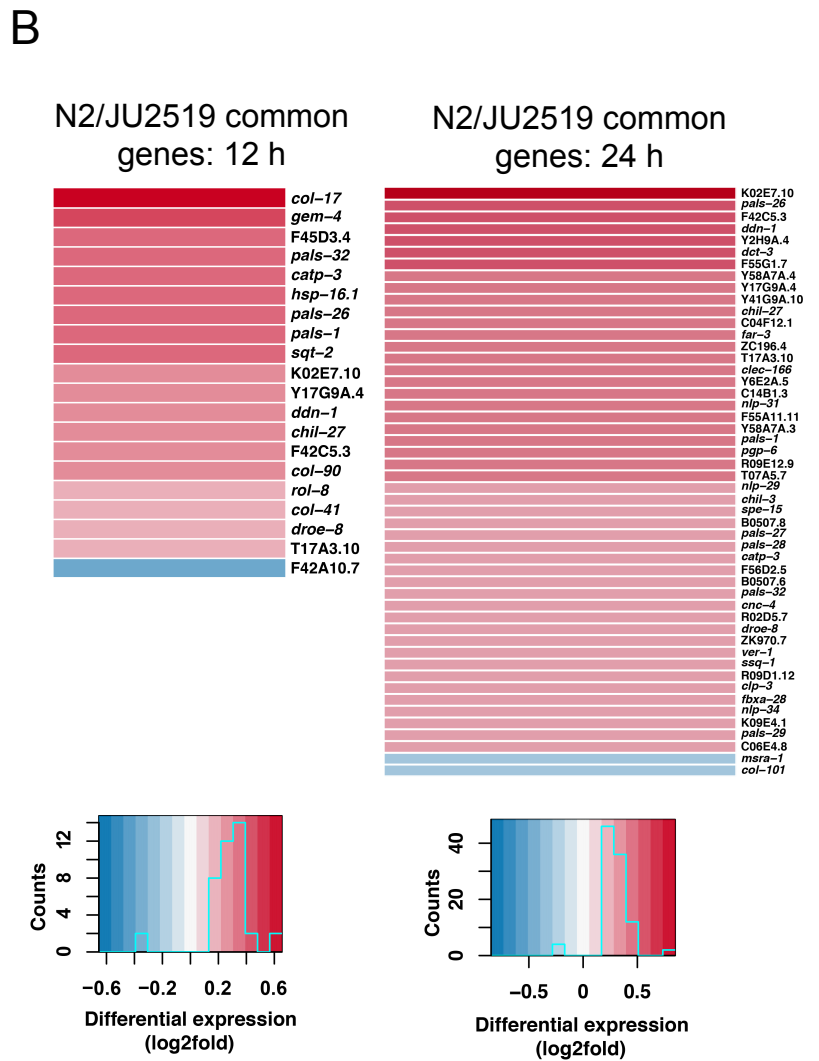
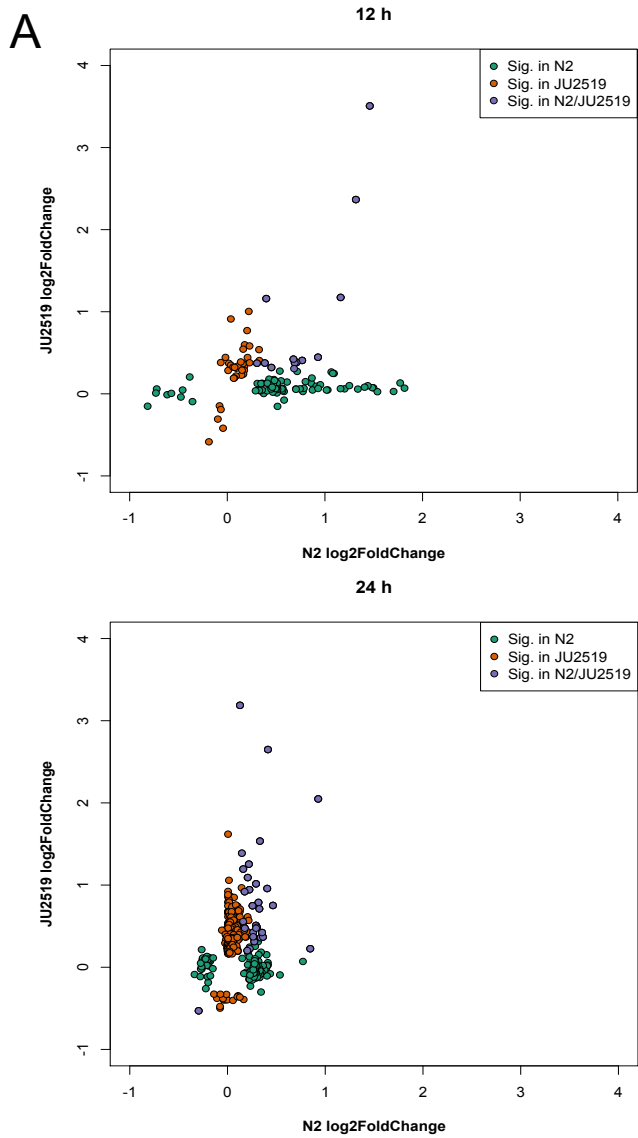


Figure S2. Gene expression changes upon exposure to *M. humicola*, related to Figure 3.

(A) Scatter plots showing the relationship between log₂ fold changes in gene expression between N2 and JU2519. Dots correspond to genes that are differentially expressed in N2 (green dots, “sig.” stands for significant), JU2519 (red) and common genes in the two isolates (purple) after 12 hours (top) and 24 hours (bottom) of exposure to *M. humicola*. Note the strain-specific response (see N2 at 12 hours and JU2519 at 24 hours) where changes in one isolate do not correlate with changes in the other. Also note that common genes tend to be more upregulated in JU2519 as opposed to N2 especially at the 24 hours timepoint. **(B)** Heatmap showing the significantly expressed genes that are common between N2 and JU2519 after 12 hours (left) or 24 hours (right) of exposure to *M. humicola*. **(C)** Neighbour-joining consensus tree showing the relationship of the 28 Wormbase-annotated CHIL proteins. Note that *chil-28* is currently annotated as a pseudogene. The sequence used in the tree corresponds to a putative functional transcript that we recovered by 3’RACE post-infection (earlier stop codon than the current annotation at the *chil-28* sequence ...5’-atattgcacttttgcacTAG). Genes that have been found in independent experiments to be upregulated post exposure to *M. humicola* are shown in green. Blue dots mark genes that are not located on chromosome II. The tree was made as in Figure S1C-D, with no outgroup. **(D)** Heat map comparing the induction of other *C. elegans* proteins containing a GH18 domain to *chil-27* induction in N2 and JU2519, at 12 and 24 hours post exposure to *M. humicola*. With regard to true chitinases (*cht-1* to *cht-4* and *lmd-4/5*), note that only *lmd-4* was significantly upregulated in JU2519 24 hours post exposure to *M. humicola*.

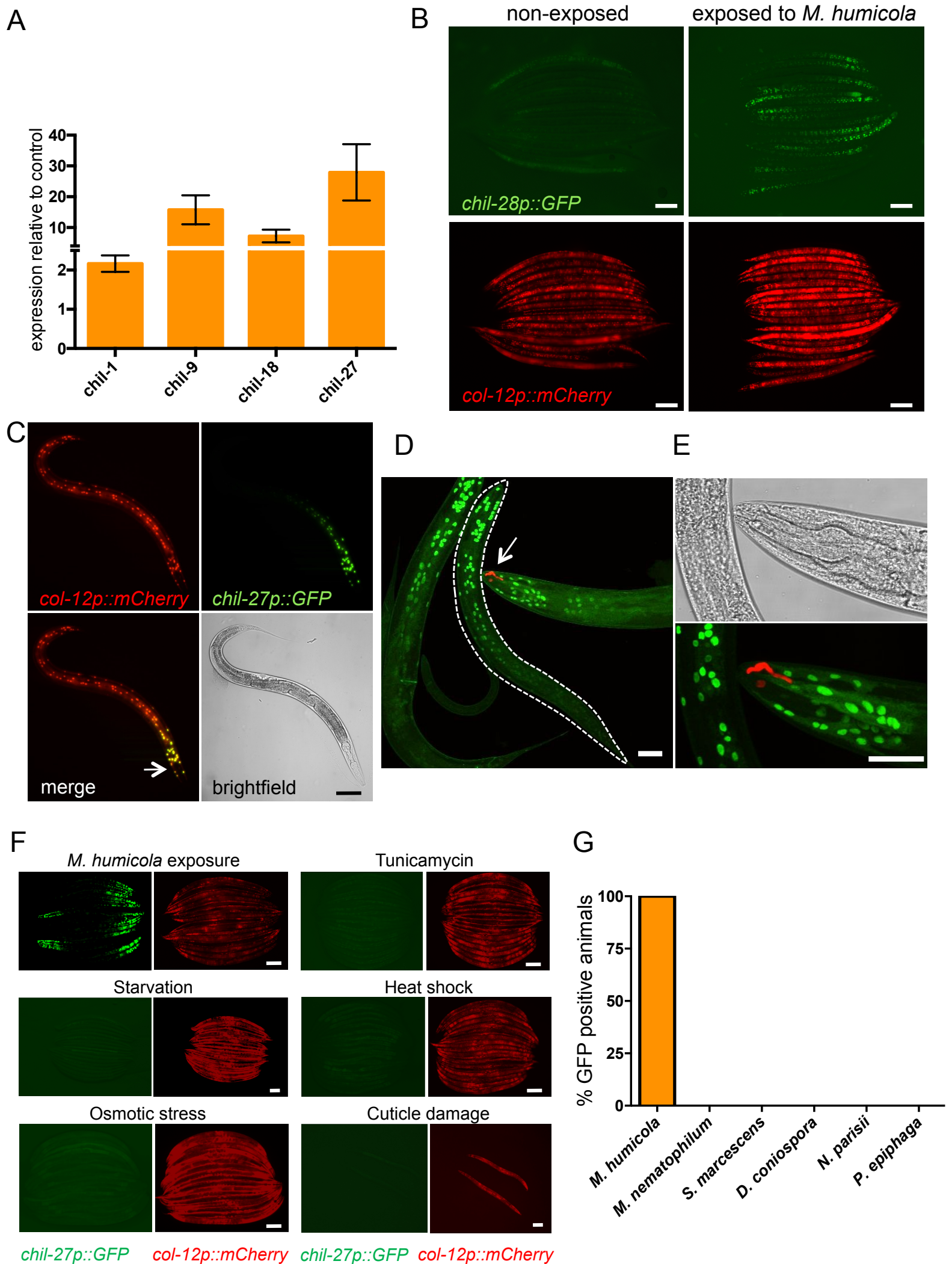


Figure S3. Induction of *chil* genes and its specificity to *M. humicola* exposure, related to Figure 3.

(A) RT-qPCR showing induction of *chil-1*, *-9*, *-18*, *-27* at 24 hours post-exposure to *M. humicola* relative to control animals that have never been exposed to the pathogen. (B) Induction of *chil-28p::GFP* post-exposure to *M. humicola*. (C) Induction of *chil-27p::GFP* in the hypodermis co-localises with the expression of the *col-12p::mCherry* marker. Note that GFP is expressed in a graded manner with stronger expression in the head region, n >100 animals. (D-E) Pathogen detection by 18S/L30 FISH (red is pathogen) in animals containing the *chil-27p::GFP* reporter that have been exposed to *M. humicola*. Note that *chil-27p::GFP* can be induced in the absence of detectable pathogen, n= 50. Only the animal on the right carries the pathogen (arrow marks the developing hypha) whereas all three animals express the reporter. The outline of a Z-stack projection of an entire animal expressing GFP is shown with a dashed line. E is a close-up of D to show the growing hypha in one of these animals. (F-G) Induction assays using *chil-27p::GFP* show specificity of induction to exposure to *M. humicola* in comparison to abiotic (F) and biotic (G) stress, n > 30 animals. Scale bars in B, C, F are 100 μ m and in D, E is 20 μ m.

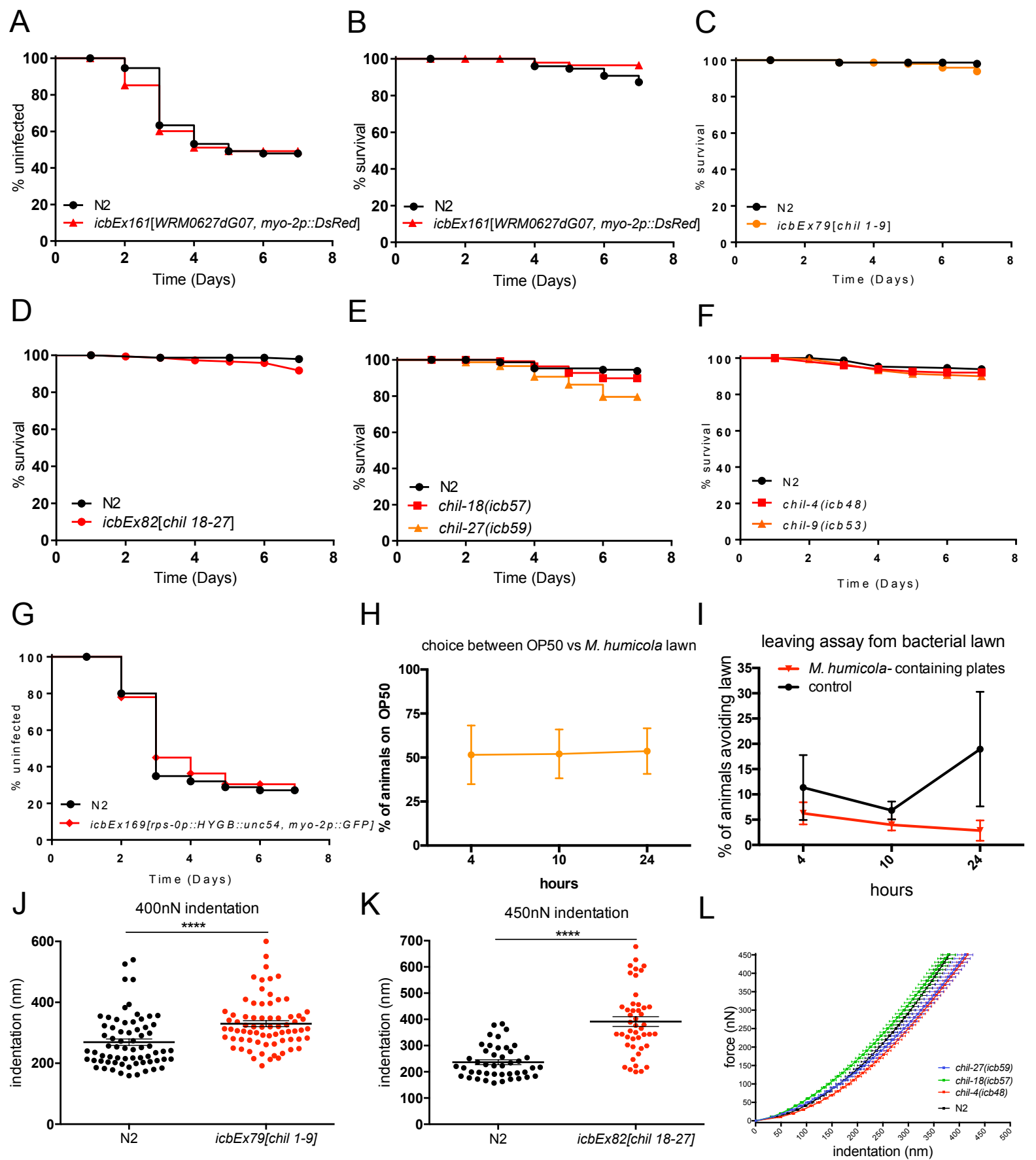


Figure S4. Control treatments, pathogen avoidance assays and force-displacement quantifications, related to Figure 4.

(A-B) Infection (A) and survival (B) assays using an unrelated fosmid (WRM0627dG07) as control. (C-F) Control survival assays for the duration of the infection assay using transgenic animals carrying fosmids containing *chil* genes 1-9 (C) and 18-27 (D) and strains carrying CRISPR knock-out mutations in *chil-4*, *chil-9* (E) and *chil-18* and *chil-27* (F). (G) Infection assay using a transgenic strain expressing the hygromycin resistance gene and *myo-2::GFP* as co-injection marker in comparison to N2 animals (H-I) Behavioural assays show no evidence for *C. elegans* avoiding bacterial lawns containing *M. humicola*. Pathogen avoidance was quantified by either monitoring whether N2 animals prefer a lawn that contains the pathogen as opposed to a lawn without the pathogen (H) or whether N2 animals are more likely to leave an OP50 lawn if this also contains the oomycete (I). (J-K) Force-displacement datasets at 400/450 nN showing pronounced indentation in transgenic animals carrying fosmids containing *chil* genes 1-9 (C) and 18-27 (D) compared to N2 animals. Stars show statistically significant changes with a T-test, **** $p < 0.0001$. (L) Force-displacement curves in strains carrying CRISPR knock-out mutations in *chil-4*, *chil-18* and *chil-27*. Note that there is no difference in stiffness among these strains.